

Thermal behavior of optical fibers during the cooling stage of the drawing process

Mohan Singh

A Dissertation Submitted to
Indian Institute of Technology Hyderabad
In Partial Fulfillment of the Requirements for
The Degree of Master of Technology



भारतीय प्रौद्योगिकी संस्थान हैदराबाद
Indian Institute of Technology Hyderabad

Department of Mechanical Engineering

August, 2011

Declaration

I declare that this written submission represents my ideas in my own words, and where others' ideas or words have been included, I have adequately cited and referenced the original sources. I also declare that I have adhered to all principles of academic honesty and integrity and have not misrepresented or fabricated or falsified any idea/data/fact/source in my submission. I understand that any violation of the above will be a cause for disciplinary action by the Institute and can also evoke penal action from the sources that have thus not been properly cited, or from whom proper permission has not been taken when needed.

Mohan Singh

(Signature)

Mohan Singh

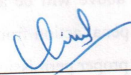
(Student Name)

ME09G009

(Roll No)


Approval Sheet

This thesis entitled **Thermal behavior of optical fibers during the cooling stage of the drawing process** by Mohan Singh is approved for the degree of Master of Technology from IIT Hyderabad.



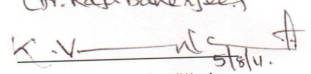
-Name and affiliation-

Examiner
Dr. Vinod Janardhan



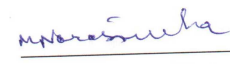
-Name and affiliation-

Examiner
Dr. Raj Banerjee



-Name and affiliation-

Adviser
Dr. K. Venkatasubbiah



-Name and affiliation-

Chairman
Dr. Narasimha Murthy

UNIC
XEROX & P
CELLULAR RESEARCH
FIBRE OPTIC PROJECT
Cell : 5482051888, 8298
BMC-17 (Dharma) Bally

Acknowledgements

I would like to express my deepest gratitude and appreciation to my Project Guide and advisor Dr. K. Venkatasubbaiah (Assistant Professor, Department of Mechanical Engineering) for his invaluable guidance, encouragement, support and understanding throughout the whole course of my M.Tech. Program. His perspicacity in my project report helped me to frame the project report in an elegant manner.

I wish to thank to all the faculty members of Mechanical Engineering Department for instilling in me a sense of self-confidence and helping me as and when I needed them. I would like to express my gratitude to all the teaching and non-teaching staff for providing the required facilities promptly.

I express my deep sense of gratitude to Almighty God for their benign blessings without which this Seminar report was not possible.

I would like to express my gratitude to my family, for their unending support, love and encouragement, which helped in overcoming hurdles and successful completion of this project. I would also like to thank all my friends for their help and support throughout the project work.

Last but not least I thank all the members of the committee for my dissertation for their comments and suggestions based on their careful evaluation of my work.

**DEDICATED
TO
MY BELOVED PARENTS**

Abstract

Thermal behavior of optical fibers during the cooling stage of the drawing process has been studied numerically. An optical fiber during the cooling stage of the drawing process can be modeled as an infinite cylinder moving in still air at a constant speed. Two-dimensional unsteady energy equation is solved using fourth order Runge-Kutta method (RK-4) for time integration and second order finite difference schemes for spatial derivatives. Two-dimensional steady boundary layer equations are solved to estimate the value of convective heat transfer coefficient at the surface of the fiber using implicit finite difference method. The velocity and temperature contours are plotted with different values of Reynolds number. The value of convective heat transfer coefficient is matching very well with the results available from the literature. Results are reported with different speed and size of the optical fiber. Reported results show that the cooling rate of the optical fiber is increases with the increase of drawing velocity at a fixed diameter. The cooling rate of the optical fiber is increases with the increase of diameter at a constant drawing velocity. The cooling rate of the optical fiber decreases with the increase of thermal conductivity for a fixed size and drawing speed of the fiber. The present results are matching very well with results available from the literature.

Nomenclature

U_f	Speed of the fiber
U	Drawing speed of the fiber
κ_f	Thermal conductivity of fiber
κ	Thermal conductivity of air
α_f	Thermal diffusivity of fiber
α	Thermal diffusivity of air
ν	Kinematic viscosity of air
h	Convective heat transfer coefficient
z	Axial distance in (z, r) plane
r	Radial distance in (z, r) plane
ξ	Axial distance in (ξ, η) plane
η	Radial distance in (ξ, η) plane
u	Axial velocity
v	Radial velocity
Z_{\max}	Maximum axial distance
R_{\max}	Maximum radial distance
D	Diameter of the fiber
T_i	Initial temperature of the fiber
T_o	Softening temperature of the glass at furnace exit
T_∞	Air temperature
T_s	Surface temperature
θ, T	Non-dimensional temperature
Re	Reynolds number
Pr	Prandtl number
Pe	Peclet number
Bi	Biot number
Nu_{avg}	Average Nusselt number
t	Time
*	Dimensional quantities

Contents

Declaration.....	Error! Bookmark not defined.
Approval Sheet	Error! Bookmark not defined.
Acknowledgements.....	iv
Abstract.....	vi
Nomenclature	vii
1 Introduction	1
1.1 Motivation.....	1
1.2 Problem statement.....	2
1.3 Literature survey	2
1.4 Objectives of present work	3
1.5 Optical fiber material selection.....	4
1.6 Advantages of glass optical fibers	4
1.7 Manufacturing of glass optical fibers.....	5
1.8 Optical fiber materials.....	7
1.9 Applications of glass optical fibers.....	8
1.10 Overview of the dissertation	8
2 Governing equation and boundary conditions	10
2.1 Mathematical modeling	10
2.2 Governing equation.....	11
2.3 Non-dimensionalization of governing equation.....	11
2.3.1 Non-dimensionalized steps.....	12
2.3.2 Non-dimensionalized parameters	12
2.3.3 Non-dimensionalized governing equation.....	13
2.4 Boudary and initial conditions	15
2.5 Non-dimensionalized numbers	17
3 Boundary layer equations	18
3.1 Boundary layer equations	18
3.1.1 Continuity equation	18
3.1.2 Momentum equation.....	19
3.1.3 Energy equation.....	19
3.2 Non-dimensionalized parameters.....	19

3.3	Non-dimensionalized boundary layer equations.....	20
3.3.1	Continuity equation.....	20
3.3.2	Momentum equation.....	20
3.3.3	Energy equation.....	20
3.4	Boundary conditions.....	21
3.5	Non-dimensionalized boundary conditions.....	21
3.6	Nusselt number.....	21
4	Numerical methods.....	22
4.1	Numerical procedure of solving boundary layer equations.....	22
4.1.1	Implicit solution of momentum boundary layer equation.....	23
4.1.2	Implicit solution of energy boundary layer equation.....	24
4.1.3	Implicit solution of continuity boundary layer equation.....	26
4.2	Numerical procedure of solving governing equation.....	27
5	Results and discussion.....	32
5.1	Convection results.....	32
5.2	Transient results.....	41
5.2.1	Validation of numerical approach.....	41
5.2.2	Selection of Z_{\max}	46
5.2.3	Effect of drawing speed and size of optical fiber.....	55
5.2.4	Effect of Bi number.....	57
5.2.5	Effect of Pe number.....	58
5.2.6	Effect of high drawing speed of fiber.....	60
5.2.7	Effect of thick fiber.....	62
5.2.8	Effect of material.....	64
5.2.9	Effect of thermal conductivity.....	71
6	Conclusions.....	75
6.1	Future work.....	76
	References.....	77

Chapter 1

Introduction

1.1 Motivation

Optical fibers are used in numerous applications in communications, biomedical, Space, hazardous environments. The drawing process of optical fibers has been the subject of numerous investigations over the past two decades. These studies were motivated by the need to improve the quality and increase the yield of optical fibers and optical multi fiber systems. The majority of the investigations have focused on the optical properties and performance of the optical fibers.

Heat transfer effects during the process play a very important role; significantly less work has been done in the area of thermal modeling of optical fiber drawing processes. Most fiber drawing speeds, furnace operating temperatures, and cooling schemes are determined by time-consuming and costly trial and error techniques. Thermal modeling of the process can provide researchers and industrial production lines with simulation tools that will assist them in process optimization and new product design. Present investigation has been motivated due to the following points. (i) Correct estimated values of convective heat transfer coefficient at the surface of the fiber are not available in the literature. (ii) Accurate numerical results do not exist in the literature for transient analysis of optical fibers during the cooling stage of the drawing process.

1.2 Problem statement

Numerical study on thermal behavior of optical fibers during the cooling stage of the drawing process

- Effect of physical parameters like speed and size of fibers:

Results for obtained for the fiber drawing speed varies from 0.5 cm/s to 1.0 m/s and size of fibers from 0.5 mm to 3.0 mm.

- Effect of the fiber material:

We compared results for two different fiber materials (VYCOR and BK7) for same physical parameters like speed and size of fiber to see the effect of fiber material.

1.3 Literature survey

Optical fibers are used in numerous applications in communications, biomedical, space, hazardous environments. The drawing process of a single fiber, a glass rod is placed in a cylindrical furnace and is heated to a softening temperature, which depends on the type of glass processed as given McLellan and Shand [1]. At that temperature the glass is soft and it can be pulled downward to form a glass fiber. As the fiber exits the furnace, it enters the cooling stage, where convection from the fiber to the air cools the fiber. In the case of thin fibers, the drawn fiber is attached to a rotating drum that winds it. In the case of thick fibers, the drawn fiber is cut in straight pieces using a glass cutting instrument. The study of thermal behavior of optical fiber during the drawing process is needed to improve the quality and increase the yield of the optical fiber.

Anderson [2] has studied the conjugate heat transfer of continuously moving surfaces. The analysis was limited to thin fibers since neglecting the axial heat conduction and assumed a constant heat transfer coefficient was used. Glicksman [3] has studied for the cooling of glass fibers. He reported results using the approximated value of convective heat transfer coefficient. Bourne and Elliston [4] studied the axially symmetric boundary layer on a moving circular fiber. They have neglected heat conduction in the axial and radial directions. Bourne and Dixon [5] studied cooling of fiber in the formation process. They have used Von Karman-Pohlhausen method to solve the boundary layer equations. They have reported the analytical model to estimate the temperature of the fiber as a function of axial distance. They have derived the expression from the steady state energy equation by neglecting radial heat conduction.

Paek and Runk [6] have studied the physical behavior of the neck down region during furnace drawing of silica fibers. Homsy and Walker [7] studied the heat transfer in laser drawing of optical fibers. Sayles and Casewell [8] have studied the neck down region of fiber drawing using the finite element analysis. Myers [9] has studied the unsteady analysis of preform drawing. He has solved the one dimensional unsteady energy equation. HarisPapamichael and Miaoulis [10] have studied thermal behavior of optical fibers during the cooling stage of drawing process. They have solved the two dimensional steady state energy equation with the Von Karman-Pohlhausen method to find the convective heat transfer coefficient. Roy Choudhury and Jaluria [11] have studied the transient temperature distribution in a moving rod or plate of finite length with surface heat transfer. They have solved the two dimensional unsteady energy equation using infinite series solution with a known value of convective heat transfer coefficient. Yin and Jaluria [12] have studied the thermal transport and material flow in high speed optical fiber drawing. The conjugate problem involving the glass and purge gas regions was solved. The zonal method was used to calculate radiative heat transfer in the glass.

1.4 Objectives of present work

In the present study our aim is twofold:

First, we focus on correct estimation of convective heat transfer coefficient (h) at the surface of the fiber:

- Develop accurate numerical method to evaluate convective heat transfer coefficient:

The boundary layer equations are solved using implicit finite difference method to evaluate convective heat transfer coefficient. For Validation; evaluated convective heat transfer coefficient value is compared to the value obtained by correlation.

Second, we focus on cooling of optical fiber with different physical parameters:

- To study the effect of speed and size of the optical fiber on cooling:

We consider speed ranging from 0.5 cm/s to 1.0 m/s and size of fibers ranging from 0.5 mm to 3mm to study the effect of speed and size of the optical fiber on cooling.

- To study the effect of material on cooling:

Comparing two different fiber materials (VYCOR and BK7) for same physical parameters like speed and size of fiber to study the effect of material, where VYCOR is high thermal conductivity material as compared to BK7.

1.5 Optical fiber material selection

Following are the basic requirements for selecting fiber materials for manufacturing optical fibers.

- The material must be transparent at particular wavelengths so that signals may be transmitted efficiently.
- The material must also be of a composition such that fibers may be drawn from it that is long, thin, and flexible.
- Materials must be used to construct the core and the cladding that can be tuned or modified to have slightly different in index of refraction, but are physically and chemically compatible.

1.6 Advantages of glass optical fiber

- **Immunity from electrical interference:** Optic fibers can run comfortably through areas of high level electrical noise such as near machinery and discharge lighting.
- **No crosstalk:** When copper cables are placed side by side for a long distance, electromagnetic radiation from each cable can be picked up by the others and so the signals can be detected on surrounding conductors. This effect is called crosstalk. In a telephone circuit it results in being able to hear another conversation in the background. Crosstalk can easily be avoided in optic fibers even if they are closely packed.
- **Glass fibers are insulators:** Being an insulator, optic fibers are safe for use in high voltage areas. They will not cause any arcing and can be connected between devices which are at different electrical potentials. The signals are carried by light and this offers some more advantages.
- **Improved bandwidths:** Using light allows very high bandwidths. Bandwidths of several gigahertz are available on fibers whereas copper cables are restricted to about 500 MHz.
- **Security:** As the optic fibers do not radiate electromagnetic signals, they offer a high degree of security.
- **Low losses:** Fibers are now available with losses as low as 0.2 dBkm⁻¹ and hence very wide spacing is possible between repeaters. This has significant cost benefits in long distance telecommunication systems, particularly for undersea operations.
- **Size and weight:** The primary coated fiber is extremely small and light, making many applications like endoscopes possible. Even when used as part of a cable with

strength members and armoring, the result is still much lighter and smaller than the copper equivalents. This provides many knock-on benefits like reduced transport costs, more cables can be fitted within existing ducts and they are easier to install.

- **Only a single fiber is required:** One fiber can send a signal whereas copper requires two wires, one of which is needed as a return path to complete the electrical circuit.

1.7 Manufacturing of glass optical fibers

Three methods are used today to fabricate moderate-to-low loss fibers: modified chemical vapor deposition (MOCVD), outside vapor deposition (OVD), and vapor axial deposition (VAD).

The production of an optical glass is still today a complex challenge; detailed compositions and technological procedures are proprietary and/or kept secret. The manufacturing of optical fiber is performed in two steps: First a preform is made. The term refers to a rod of glass, typically 1m long, with a diameter of 10–50 mm, and with the refractive index profile already built into it. In the second step, this preform is then softened by heating and stretched out by pulling so that the final fiber is obtained.

The drawing process of a single fiber, a glass rod is placed in a cylindrical furnace and is heated to a softening temperature, which depends on the type of glass processed as given McLellan and Shand [1]. At that temperature the glass is soft and it can be pulled downward to form a glass fiber. As the fiber exits the furnace, it enters the cooling stage, where convection from the fiber to the air cools the fiber. In the case of thin fibers, the drawn fiber is attached to a rotating drum that winds it. In the case of thick fibers, the drawn fiber is cut in straight pieces using a glass cutting instrument.

The heating, along with the extensional deformation caused by the draw tension, gives rise to the “neck-down” profile inside the furnace. The neck-down shape depends on the drawing conditions as well as on the physical and process variables. It is within this region that the index of refraction profile may be altered, thus affecting the optical bandwidth of the fiber. Also the defect concentration within the fiber is dependent on the thermal transport and glass flow in this neck-down region, as discussed by Hanafusa et al. [13].

This extreme heat causes two chemical reactions to happen:

- The silicon and germanium react with oxygen, forming silicon dioxide (SiO₂) and germanium dioxide (GeO₂).
- The silicon dioxide and germanium dioxide deposit on the inside of the tube and fuse together to form glass.

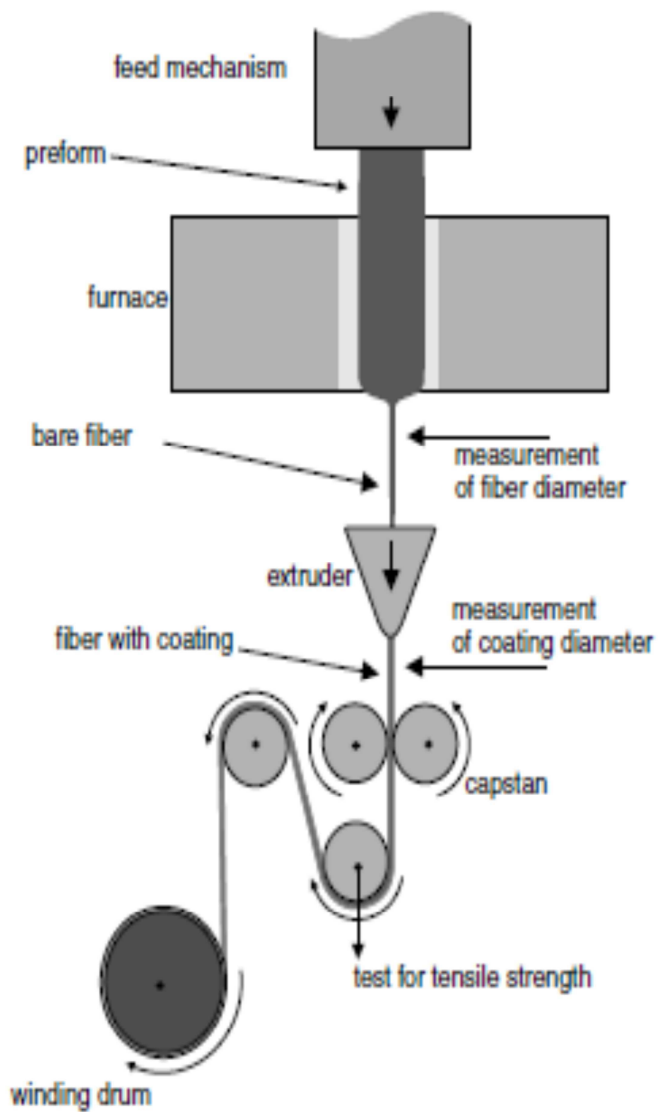
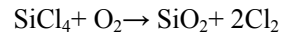
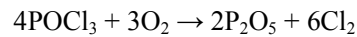
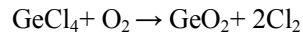


Figure 1.1: Optical fiber process [14]

Standard dopants for silica fiber include GeO_2 , P_2O_5 , B_2O_3 , and SiF_4 . The former two are used to increase the refractive index (and are therefore used in the core), while the latter decrease the index of refraction (and are therefore used in the cladding). The most frequently used dopant is germanium. Dopants are added through their chlorides to the reaction gas, and there can be the following reaction:



1.8 Optical fiber materials

The most commonly used optical materials are fused silica, VYCOR and Schott BK7

- Schott Bk-7 optical glass:** Borosilicate glass Schott BK7 is an extremely common crown glass, used in precision lenses. Borosilicate contains about 10% boric oxide, have good optical and mechanical characteristics, and are resistant to chemical and environmental damage. It has a high transmission and is free of bubbles and inclusions. Since BK7 performs well in all chemical tests, no special handling is required, thus reducing manufacturing costs. It is a relatively hard material with extremely low bubble and inclusion content. BK7 provides excellent transmittance through-out the visible and near infrared spectra and down to 350 nm in the ultraviolet.

Composition: $\text{SiO}_2=69.13\%$ $\text{B}_2\text{O}_3=10.75\%$ $\text{BaO}=3.07\%$ $\text{Na}_2\text{O}=10.40\%$ $\text{K}_2\text{O}=6.29\%$ $\text{As}_2\text{O}_3=0.36\%$

- VYCOR code 7913:** VYCOR is a glass with high temperature and thermal shock resistance, made by Corning Incorporated. VYCOR is 96% silica, but unlike pure fused silica it can be readily manufactured in a variety of shapes. Special Properties are Low thermal expansion, High temperature resistance, High temperature change resistance, Low specific weight, Heat resistant 96% silica glass, Good chemical resistance.

Composition: $\text{SiO}_2=96.4\%$ $\text{B}_2\text{O}_3=3.0\%$ $\text{Al}_2\text{O}_3=0.5\%$ Misc. Traces=0.1%

Properties of optical fiber materials are shown in Table 1.1. Data is collected from Handbook of optical materials [19].

Table 1.1 Comparisons of properties of optical materials

Material	BK7	VYCOR
Density (g/cm³)	2.51	2.18
Specific Heat (J/kg-K)	858	750
Thermal Conductivity (W/m-k)	1.114	1.38
Thermal Diffusivity (m²/s)*10⁻⁶	0.5172782	0.8440367

1.9 Applications of glass optical fiber

Glass optical fibers have a large area of applications. Some of them are following:

- **Telecommunication:** Telecommunication applications are widespread, ranging from global networks to desktop computers. These involve the transmission of voice, data, or video over distances of less than a meter to hundreds of kilometers, using one of a few standard fiber designs in one of several cable designs.
- **Transmission of data:** Optical fiber is also used extensively for transmission of data. The high bandwidth provided by fiber makes it the perfect choice for transmitting broadband signals, such as high-definition television (HDTV) telecasts.
- **Intelligent transportation systems:** Intelligent transportation systems, such as smart highways with intelligent traffic lights, automated tollbooths, and changeable message signs, also use fiber-optic-based telemetry systems.
- **Biomedical industry:** Another important application for optical fiber is the biomedical industry. Fiber-optic systems are used in most modern telemedicine devices for transmission of digital diagnostic images.
- **Other applications:** Other applications for optical fiber include space, military, automotive, and the industrial sector.

1.10 Overview of the dissertation

The remainder of this dissertation is organized as follows:

- Chapter 2 deals with the governing equation of two dimensional unsteady energy equation with boundary and initial conditions. The non-dimensional form of energy equation is also given.
- Chapter 3 deals dimensional and dimensionless form of steady boundary layer equations with boundary conditions

- Chapter 4 discusses the numerical methods to solve the energy equation and boundary layer equations
- Chapter 5 discusses the results of thermal behavior of optical fibers with different physical parameters.
- Chapter 6 discusses the summary and conclusions of the present study.
- Figures and tables are placed where they were cited first.

Chapter 2

Governing equation and boundary conditions

2.1 Mathematical modeling

An optical fiber during the cooling stage of the drawing process can be modeled as an infinite cylinder moving in still air at constant speed.

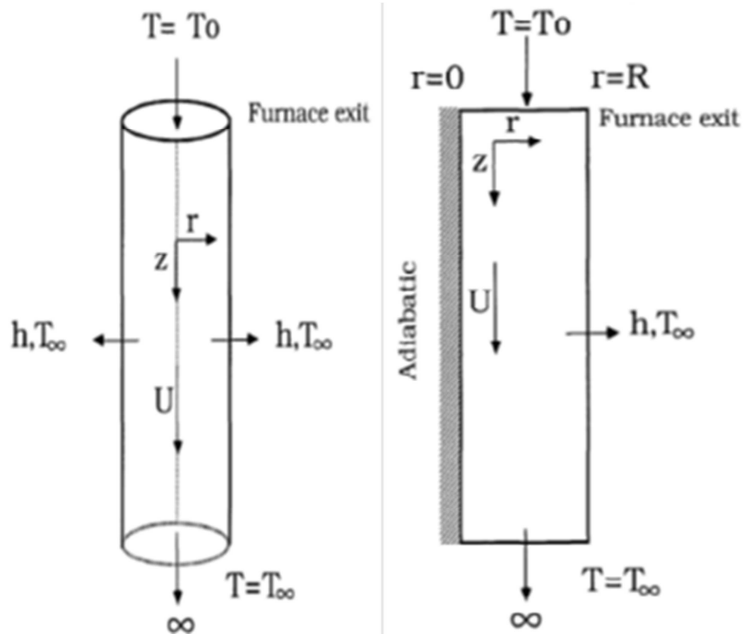


Figure 2.1: Thermal model of optical fiber with boundary conditions [10]

2.2 Governing equation

Consider 2-dimensional unsteady heat conduction in a cylindrical rod moving at a constant speed in still air. The governing energy equation is written in dimensional form (indicated by the quantities with asterisk) with the assumption of constant material properties and is given by;

$$\frac{\partial T^*}{\partial t^*} + U_f \frac{\partial T^*}{\partial z^*} = \alpha_f \left(\frac{1}{r^*} \frac{\partial T^*}{\partial r^*} + \frac{\partial^2 T^*}{\partial r^{*2}} + \frac{\partial^2 T^*}{\partial z^{*2}} \right) \quad (1)$$

$$\left(\frac{1}{r^*} \frac{\partial T^*}{\partial r^*} + \frac{\partial^2 T^*}{\partial r^{*2}} \right) = \text{Radial heat conduction in fiber}$$

$$\left(\frac{\partial^2 T^*}{\partial z^{*2}} \right) = \text{Axial heat conduction}$$

$$U_f \frac{\partial T^*}{\partial z^*} = \text{Heat transferred due to motion of the fiber}$$

r = Radial distance

z = Axial distance

U_f = Drawing speed of the fiber

α_f = Thermal diffusivity

T^* = Temperature of the fiber

2.3 Non-dimensionalization of governing equation

Non-dimensionalization is the partial or full removal of units from a mathematical equation by a suitable substitution of variables. This technique can simplify and parameterize problems where measured units are involved. It is closely related to dimensional analysis. In some physical systems, the term scaling is used interchangeably with non dimensionalization, in order to suggest that certain quantities intrinsic to the system, rather than units such as SI units. Non-dimensionalization is not the same as converting extensive quantities in an equation to intensive quantities, since the latter procedure results in variables that still carry units.

Dimensional analysis is based on the principle that all additive or equated terms of a complete relationship between the variables must have the same net dimensions. The analysis starts with the preparation of a list of individual dimensional variables (dependant, independent and parametric) that are presumed to define the behavior of interest. The performance of dimensional analysis in this context is reasonably simple and straightforward; the principle difficulty and uncertainty arise from the identification of variables to be included or excluded.

2.3.1 Non-dimensionalized steps

To non-dimensional a system of equation, one must do the following:

- Identify all the independent and dependent variables;
- Replace each of them with a quantity scaled relative to a characteristic unit of measure to be determined;
- Divide through by the coefficient of the highest order polynomial or derivative term.
- Choose judiciously the definition of characteristics unit for each variable so that the coefficients of as many terms as possible become 1;
- Rewrite the system of equations in terms of their new dimensionless equations.
- The last three steps are usually specific to the problem where non-dimensionalization is applied. However, almost all systems require the first two steps to be performed.

2.3.2 Non-dimensionalized parameters

- A dimensionless special radial coordinate may be defined as:

$$r = \frac{r^*}{D}$$

- A dimensionless special axial coordinate may be defined as:

$$z = \frac{z^*}{D}$$

- A dimensionless time may be defined as:

$$t = \frac{\alpha_f t^*}{D^2}$$

- A dimensionless temperature may be defined as:

$$\theta = \left(\frac{T^* - T_\infty}{T_i - T_\infty} \right)$$

Where D is the diameter of the fiber, T_i initial temperature of the fiber, T_∞ is the air temperature.

2.3.3 Non-dimensionalized governing equation

The governing unsteady state energy equation in z, r plane is given by:

$$\left(\frac{\rho_f c_f}{\kappa_f} \right) \frac{\partial T^*}{\partial t^*} + U_f \left(\frac{\rho_f c_f}{\kappa_f} \right) \frac{\partial T^*}{\partial z^*} = \left(\frac{1}{r^*} \frac{\partial T^*}{\partial r^*} + \frac{\partial^2 T^*}{\partial r^{*2}} + \frac{\partial^2 T^*}{\partial z^{*2}} \right)$$

$$\frac{\partial T^*}{\partial t^*} + U_f \frac{\partial T^*}{\partial z^*} = \alpha_f \left(\frac{1}{r^*} \frac{\partial T^*}{\partial r^*} + \frac{\partial^2 T^*}{\partial r^{*2}} + \frac{\partial^2 T^*}{\partial z^{*2}} \right)$$

By using non-dimensionalized parameters;

$$\frac{\partial T^*}{\partial t^*} = \alpha_f \frac{\partial \theta}{\partial t} \left(\frac{T_i - T_\infty}{D^2} \right)$$

$$\frac{\partial T^*}{\partial z^*} = \frac{\partial \theta}{\partial z} \left(\frac{T_i - T_\infty}{D} \right)$$

$$\frac{\partial T^*}{\partial r^*} = \frac{\partial \theta}{\partial r} \left(\frac{T_i - T_\infty}{D} \right)$$

$$\frac{\partial^2 T^*}{\partial r^{*2}} = \frac{\partial^2 \theta}{\partial r^2} \left(\frac{T_i - T_\infty}{D^2} \right)$$

$$\frac{\partial^2 T^*}{\partial z^{*2}} = \frac{\partial^2 \theta}{\partial z^2} \left(\frac{T_i - T_\infty}{D^2} \right)$$

The governing non-dimensional energy equation in z, r plane is given by:

$$\begin{aligned} \alpha_f \frac{\partial \theta}{\partial t} \left(\frac{T_i - T_\infty}{D^2} \right) + U_f \frac{\partial \theta}{\partial z} \left(\frac{T_i - T_\infty}{D} \right) \\ = \alpha_f \left[\frac{1}{rD} \frac{\partial \theta}{\partial r} \left(\frac{T_i - T_\infty}{D} \right) + \frac{\partial^2 \theta}{\partial r^2} \left(\frac{T_i - T_\infty}{D^2} \right) + \frac{\partial^2 \theta}{\partial z^2} \left(\frac{T_i - T_\infty}{D^2} \right) \right] \end{aligned}$$

Divide the equation from term $\left(\frac{T_i - T_\infty}{D^2} \right) \alpha_f$

$$\frac{\partial \theta}{\partial t} + U_f \frac{\partial \theta}{\partial z} \left(\frac{D}{\alpha_f} \right) = \left(\frac{1}{r} \frac{\partial \theta}{\partial r} + \frac{\partial^2 \theta}{\partial r^2} + \frac{\partial^2 \theta}{\partial z^2} \right)$$

$$\frac{\partial \theta}{\partial t} + \left(\frac{U_f D}{\alpha_f} \right) \frac{\partial \theta}{\partial z} = \left(\frac{1}{r} \frac{\partial \theta}{\partial r} + \frac{\partial^2 \theta}{\partial r^2} + \frac{\partial^2 \theta}{\partial z^2} \right)$$

$$\frac{\partial \theta}{\partial t} + Pe \frac{\partial \theta}{\partial z} = \left(\frac{1}{r} \frac{\partial \theta}{\partial r} + \frac{\partial^2 \theta}{\partial r^2} + \frac{\partial^2 \theta}{\partial z^2} \right)$$

Finally governing equation can be written as:

$$\frac{\partial \theta}{\partial t} = -Pe \frac{\partial \theta}{\partial z} + \left(\frac{\partial^2}{\partial r^2} + \frac{\partial^2}{\partial z^2} \right) \theta + \frac{1}{r} \frac{\partial \theta}{\partial r} \quad (2)$$

The Governing equation is transformed from (z, r) coordinates to (ξ , η) coordinates for higher resolution in the axial direction. The transformation from (z, r) to (ξ , η) is given by:

$$z(\xi) = z_{\max} \left[1 - \frac{\tanh[\beta_1(1 - \xi)]}{\tanh \beta_1} \right] \quad (3)$$

$$r(\eta) = \eta \quad (4)$$

Where $\beta_1 = 2.0$ is used to obtain a grid clustering near the furnace exit in the axial direction. z_{\max} is the maximum axial distance.

Orthogonal grids are preferred for the following reasons; Simpler transformed equations and their differenced form, Accurate and easy implement of boundary conditions, smaller numerical errors of the solutions for governing differential equations by faster methods. The accuracy and the speed of method could be due to mapping. Orthogonal grid is optimum choice between complete non-orthogonal grids and conformal mapping.

The governing non-dimensionalization equation in transformed plane is given by:

$$\frac{\partial \theta}{\partial t} = -\text{Pe} \frac{1}{h_1} \frac{\partial \theta}{\partial \xi} + \frac{1}{h_1} \left[\frac{\partial}{\partial \xi} \left(\frac{1}{h_1} \frac{\partial \theta}{\partial \xi} \right) + \frac{\partial}{\partial \eta} \left(h_1 \frac{\partial \theta}{\partial \eta} \right) \right] + \frac{1}{\eta} \frac{\partial \theta}{\partial \eta} \quad (5)$$

Where

$$\frac{\partial \theta}{\partial z} = \frac{1}{h_1} \frac{\partial \theta}{\partial \xi}$$

$$\frac{\partial \theta}{\partial r} = \frac{\partial \theta}{\partial \eta}$$

$$\left(\frac{\partial^2 \theta}{\partial r^2} + \frac{\partial^2 \theta}{\partial z^2} \right) = \frac{1}{h_1} \left[\frac{\partial}{\partial \xi} \left(\frac{1}{h_1} \frac{\partial \theta}{\partial \xi} \right) + \frac{\partial}{\partial \eta} \left(h_1 \frac{\partial \theta}{\partial \eta} \right) \right]$$

$h_1 =$ Scale factor

$$\text{Pe} = \frac{U_f D}{\alpha_f} = \text{Peclet Number}$$

2.4 Boundary and initial conditions

A Cylindrical rod of fiber is moving with a constant speed in the axial direction. The temperature profile much varies in the axial direction compared to radial direction. Hence, temperature profile in the fiber is assumed as axisymmetric.

The governing equation (5) is solved in half of the fiber with the boundary and initial conditions given below.

- At the exit of the furnace the fiber has a uniform temperature T_0 which is the softening of the glass:

$$\text{At } z^* = 0: T^*(r^*, 0) = T_0; \quad \theta(\eta, 0) = 1.0 \quad (6)$$

- At an infinite distance from the exit of the furnace the temperature of the fiber is that of the ambient:

$$\text{At } z^* = \infty: T^*(r^*, \infty) = T_\infty; \quad \theta(\eta, z_{\max}) = 0 \quad (7)$$

- The temperature profile is axisymmetric means an adiabatic boundary condition in the center of the fiber which implies that the temperature gradient at this point is zero.

$$\text{At } r^* = \eta = 0: \frac{\partial T^*}{\partial r^*} = \frac{\partial \theta}{\partial \eta} = 0 \quad (8)$$

When the fiber exits from the furnace it is forced convective cooling due to the motion of fiber in still air. Radiation effects can be neglected due to the emissivity of glass is very low.

The convective boundary condition at the fiber surface:

$$\text{At } r^* = R: -\kappa_f \frac{\partial T^*}{\partial r^*} = h(T^* - T_\infty) \quad (9)$$

The above convective boundary condition in non-dimensional form at the surface is given by:

$$\eta = 0.5: \frac{\partial \theta}{\partial \eta} = -\text{Bi}\theta \quad (10)$$

Where R and κ_f are the radius and thermal conductivity of fiber; h is the convection heat transfer coefficient;

$$\text{And Bi} = \frac{h \cdot D}{\kappa_f} = \text{Biot Number}$$

The steady boundary layer equations of air around the fiber are solved to find the temperature profiles around the fiber. The average convective heat transfer coefficient is obtained from the boundary layer solution and it is used in equation (10).

- The initial condition is equal to the temperature of fiber at the furnace exit:

$$\text{At } t^* = t = 0: T^* = T_i = T_0; \theta = 1.0$$

(11)

2.5 Non-dimensionalized numbers

Here, non-dimensionalized numbers having significant importance in this research are discussed and more details can be found in Incropera DeWitt. [15].

- **Biot number:** A small Biot number represents small resistance to heat conduction, and thus small temperature gradients within the body. Since the Biot number is the ratio of the convection at the surface to conduction within the body.

The magnitude of the maximum temperature difference within the body depends strongly on the ability of surrounding medium to convection this heat away from the surface. The Biot number is a measure of the relative magnitudes of these two competing effects.

$$Bi = \frac{\text{Convection of the surface of the body}}{\text{Conduction within the body}}$$

- **Prandtl number:** The Prandtl number is defined as the ratio of momentum diffusivity (Kinematic viscosity, ν) and thermal diffusivity (α). It is a dimensionless number.

$$Pr = \frac{\text{Momentum Diffusivity}}{\text{Thermal Diffusivity}}$$

- **Reynolds number:** The Reynolds number is a measure of ratio of inertia forces to viscous forces and, consequently, it quantifies the relative importance of two types of forces for given flow conditions.

$$Re = \frac{\text{Inertia forces}}{\text{Viscous Forces}}$$

- **Peclet number:** Peclet number is the product of Reynolds number and Prandtl number.

$$Pe = RePr$$

Chapter 3

Boundary layer equations

3.1 Boundary layer equations

The fiber moves in the axial direction as it exits the furnace at a constant speed(U_f). At large distance from the fiber, the air is at rest which it has a temperature (T_∞). The equations describing the problem are obtained by invoking boundary layer approximation to the conservation equations. The steady boundary layer equations are written in dimensional form (indicated by the quantities with asterisk) for the velocity and temperature fields as given in White [16].

As per the boundary layer approximation:

The normal velocity(v^*) is very less compared to axial velocity(u^*).

$$(v^*) \ll (u^*)$$

$$\frac{\partial^2 u}{\partial r^2} \gg \frac{\partial^2 u}{\partial z^2}$$

$$\frac{\partial^2 T}{\partial r^2} \gg \frac{\partial^2 T}{\partial z^2}$$

3.1.1 Continuity equation

The continuity equation is essentially the equation for the conservation of mass that is the matter neither may create nor may destroyed. It is derived by taking a mass balance on the fluid entering and leaving a volume element in flow field. The continuity equation is a mathematical statement that, in any steady state process, the rate at which mass enters a system is equal to the rate at which mass leaves the system.

$$\frac{\partial u^*}{\partial z^*} + \frac{1}{r^*} \frac{\partial}{\partial r^*} (r^* v^*) = 0 \quad (12)$$

3.1.2 Momentum equation

The momentum equations are derived from Newton's second law of motion. This law requires that the sum of all forces acting on the control volume must equal the rate of increase of fluid momentum within the control volume, or in other words, the mass times the acceleration in a given direction is equal to the external forces acting on the control volume in the same direction. The external forces acting on a fluid particle are of two types body forces which are proportional to the volume and which act on the fluid particle from an external force field such as the gravitational, electric, magnetic and centrifugal fields; and the surface forces which are proportional to area and which result from the stresses such as static pressure and viscous stresses on surface of the volume element. The steady velocity boundary layer equation is given by:

$$u^* \frac{\partial u^*}{\partial z^*} + v^* \frac{\partial u^*}{\partial r^*} = \nu \frac{1}{r^*} \frac{\partial}{\partial r^*} \left[r^* \frac{\partial u^*}{\partial r^*} \right] \quad (13)$$

3.1.3 Energy equation

The energy equation can be derived by applying the first law of thermodynamics to a differential control volume in flow field. The temperature distribution equation in the flow field can be obtained by solving this set of equations subject to appropriate boundary conditions. The steady thermal boundary layer equation is given by:

$$u^* \frac{\partial T^*}{\partial z^*} + v^* \frac{\partial T^*}{\partial r^*} = \alpha \frac{1}{r^*} \frac{\partial}{\partial r^*} \left[r^* \frac{\partial T^*}{\partial r^*} \right] \quad (14)$$

Where u and v are the axial and radial velocity components; r is the radial distance from the center of the fiber; z is the fiber axial distance; ν and α are the kinematic viscosity and thermal diffusivity of the air.

3.2 Non-dimensionalized parameters

The above boundary layer equations are non-dimensionalized using the following variables.

- A dimensionless special radial coordinate may be defined as:

$$r = \frac{r^*}{D}$$

- A dimensionless special axial coordinate may be defined as:

$$z = \frac{z^*}{D}$$

- A dimensionless axial velocity component may be defined as:

$$u = \frac{u^*}{U_f}$$

- A dimensionless radial velocity component may be defined as:

$$v = \frac{v^*}{U_f}$$

- A dimensionless temperature may be defined as:

$$T = \left(\frac{T^* - T_\infty}{T_s - T_\infty} \right)$$

Where

T_s = Surface temperature of the fiber.

T = Non-dimensionalized temperature of the air.

3.3 Non-dimensionalized boundary layer equations

The non-dimensional forms of the boundary layer equations for velocity and temperature fields are given by:

3.3.1 Continuity equation

$$\frac{\partial u}{\partial z} + \frac{1}{r} \frac{\partial}{\partial r} (r v) = 0 \tag{15}$$

3.3.2 Momentum equation

$$u \frac{\partial u}{\partial z} + v \frac{\partial u}{\partial r} = \frac{1}{Re} \frac{1}{r} \frac{\partial}{\partial r} \left[r \frac{\partial u}{\partial r} \right] \tag{16}$$

3.3.3 Energy equation

$$u \frac{\partial T}{\partial z} + v \frac{\partial T}{\partial r} = \frac{1}{RePr} \frac{1}{r} \frac{\partial}{\partial r} \left[r \frac{\partial T}{\partial r} \right] \tag{17}$$

Where

$$\text{Re} = U_f \frac{D}{\nu} = \text{Reynolds number}$$

$$\text{Pr} = \frac{\nu}{\alpha} = \text{Prandtl number}$$

3.4 Boundary conditions

The boundary conditions for the above equations are taken at the surface of the fiber and at a large distance from its surface:

$$\text{At } r^* = R: u^* = U_f; v^* = 0; T^* = T_s \quad (18)$$

$$\text{At } r^* = \infty: u^* = v^* = 0; T^* = T_\infty \quad (19)$$

3.5 Non-dimensionalized boundary conditions

The boundary conditions in non-dimensional form are given by:

$$\text{At } r = 0.5: u = 1.0; v = 0; T = 1.0 \quad (20)$$

$$\text{At } r = \infty: u = v = T = 0 \quad (21)$$

Where R = Radius of the fiber

3.6 Nusselt number

The heat transfer between the fiber surface and surroundings fluid is calculated in the form of a non-dimensional number, the Nusselt number. The local Nusselt number (Nu_l) is calculated using the following equation:

$$\text{Nu}_l = -\frac{\partial T}{\partial r} \quad (22)$$

The average Nusselt number (Nu_{avg}) is obtained by integrating the local Nusselt number along the surface of the fiber:

$$\text{Nu}_{\text{avg}} = \frac{hD}{\kappa} = -\frac{1}{z_{\text{max}}} \int_0^{z_{\text{max}}} \frac{\partial T}{\partial r} dz \quad (23)$$

Where κ is the thermal conductivity of air; h is the average convective heat transfer coefficient.

Chapter 4

Numerical methods

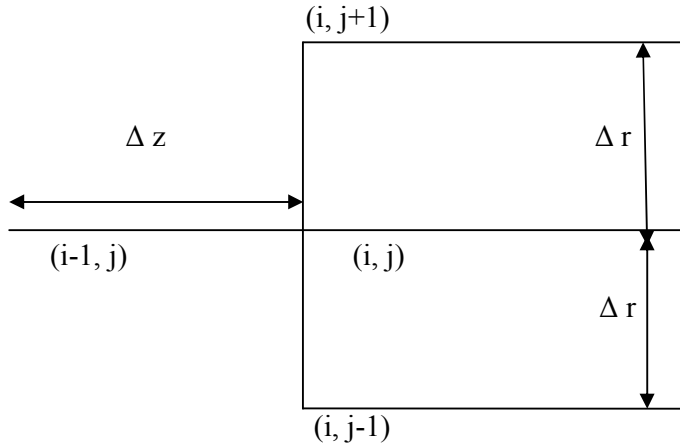
4.1 Numerical procedure of solving boundary layer equations

The boundary layer equations (15) to (17) are solved using implicit finite difference method. Here the concept of implicit finite difference method is discussed and more details can be found in Oosthizen and Naylor [17]. The boundary layer equations (15) to (17) are parabolic in z , so the numerical models are in the downstream marching type. There are two types of marching scheme: explicit and implicit. Second order finite difference scheme is used to the derivative terms in the equations (15) to (17), a set of algebraic equations obtained. The set of variables u , v and T are known at nodal points on one r -grid line, then the variables at the nodal points on the next r -grid line is obtained. The same procedure can be used to determine the variables on the r -line and so on, the solution advancing from grid line to grid line in the z direction. In the explicit scheme, the values of the variables at the point under consideration are directly determined from conditions at the points on the preceding line. In the implicit scheme, the values of the variables at adjacent points on the line on which the solution is being sought are related to each other and to the values of the variables on the preceding line. By considering each nodal point in turn on the line to which the solution advancing, a set of equations obtained which must be simultaneously solved using Thomas algorithm to obtain the values at all nodal points. In an explicit scheme, it is possible for the solution to become unstable. In order to avoid numerical instability, here implicit finite difference method is used. The temperature solution is used to obtain the average convective heat transfer coefficient (h) using the equation (23).

Here, $z_{\max} = 15$ with 1500 grid points distributed non-uniformly in the axial direction and $R_{\max} = 4.5$ with 300 points equally divided in the radial direction is used. A constant Prandtl number ($Pr = 0.7$) was used for air.

4.1.1 Implicit solution of momentum boundary layer equation

In order to express the Non-dimensionalization of governing equations (momentum and energy) using implicit scheme we follow the following procedure:



Consider first the finite difference approximation for $\frac{\partial u}{\partial r}$ at the point i, j . In order to derive finite difference approximation it is noted that the values of u at points $i, j+1$ and $i, j-1$ can be related to the value at point i, j by Taylor expressions, higher terms being ignored.

$$\frac{\partial u}{\partial r} (i, j) = \frac{u_{i, j+1} - u_{i, j-1}}{2 \cdot \Delta r}$$

Therefore second order derivative in r -direction:

$$\frac{\partial^2 u}{\partial z^2} = \frac{u_{i, j+1} + u_{i, j-1} - 2 \cdot u_{i, j}}{\Delta r^2}$$

z -derivatives are approximated to a lower order in Δz than the r -derivatives are in Δr . Then the following backward difference approximation in the z -direction will be used.

$$\frac{\partial u}{\partial z} (i, j) = \frac{u_{i, j} - u_{i-1, j}}{\Delta z}$$

Considering momentum boundary layer equation:

$$u \frac{\partial u}{\partial z} + v \frac{\partial u}{\partial r} = \frac{1}{\text{Re}} \left[\frac{\partial^2 u}{\partial r^2} + \frac{1}{r} \cdot \frac{\partial u}{\partial r} \right]$$

And

$$u \frac{\partial u}{\partial z} (i, j) = u_{i-1, j} \left(\frac{u_{i, j} - u_{i-1, j}}{\Delta z} \right)$$

$$v \frac{\partial u}{\partial r} (i, j) = v_{i-1, j} \left(\frac{u_{i, j+1} - u_{i, j-1}}{2 \cdot \Delta r} \right)$$

Finally the momentum equation can be arranged in the following form:

$$A_j u_{i, j-1} + B_j u_{i, j} + C_j u_{i, j+1} = D_j \quad i \leq 1 \leq N$$

(24)

Where

$$A_j = \left(\frac{1}{2r\Delta r} \right) - \left(\frac{1}{\text{Re}\Delta r^2} \right) - \left(\frac{v_{i-1, j}}{2\Delta r} \right)$$

$$B_j = \left(\frac{u_{i-1, j}}{\Delta z} \right) + \left(\frac{2}{\text{Re}\Delta r^2} \right)$$

$$C_j = \left(\frac{v_{i-1, j}}{2\Delta r} \right) - \left(\frac{1}{\text{Re}\Delta r^2} \right) - \left(\frac{1}{2r\Delta r} \right)$$

$$D_j = \left(\frac{u_{i-1, j}^2}{\Delta z} \right)$$

Now we can apply the Thomas algorithm for momentum equation.

4.1.2 Implicit solution of energy boundary layer equation

Consider first the finite difference approximation for $\frac{\partial T}{\partial r}$ at the point i, j . In order to derive finite difference approximation it is noted that the values of u at points $i, j+1$ and $i, j-1$ can be related to the value at point i, j by Taylor expressions, higher terms being ignored.

$$\frac{\partial T}{\partial r} (i, j) = \frac{T_{i, j+1} - T_{i, j-1}}{2\Delta r}$$

Therefore second order derivative in r-direction:

$$\frac{\partial^2 T}{\partial z^2} = \frac{T_{i, j+1} + T_{i, j-1} - 2 T_{i, j}}{\Delta r^2}$$

z-derivatives are approximated to a lower order in Δz then the r-derivatives are in Δr . Then the following backward difference approximation in the z-direction will be used.

$$\frac{\partial T}{\partial z}(i, j) = \frac{T_{i, j} - T_{i-1, j}}{\Delta z}$$

Considering energy boundary layer equation:

$$u \frac{\partial T}{\partial z} + v \frac{\partial T}{\partial r} = \frac{1}{\text{RePr}} \left(\frac{\partial^2 T}{\partial r^2} + \frac{1}{r} \cdot \frac{\partial T}{\partial r} \right)$$

And

$$u \frac{\partial T}{\partial z}(i, j) = u_{i-1, j} \left(\frac{T_{i, j} - T_{i-1, j}}{\Delta z} \right)$$

$$v \frac{\partial T}{\partial r}(i, j) = v_{i-1, j} \left(\frac{T_{i, j+1} - T_{i, j-1}}{2 \cdot \Delta r} \right)$$

Finally the energy equation can be arranged in the following form:

$$E_j T_{i, j-1} + F_j T_{i, j} + G_j T_{i, j+1} = H_j \quad i \leq 1 \leq N$$

(25)

Where

$$E_j = \left(\frac{1}{2r\Delta r} \right) - \left(\frac{1}{\text{RePr}\Delta r^2} \right) - \left(\frac{v_{i-1, j}}{2\Delta r} \right)$$

$$F_j = \left(\frac{u_{i-1, j}}{\Delta z} \right) + \left(\frac{2}{\text{RePr}\Delta r^2} \right)$$

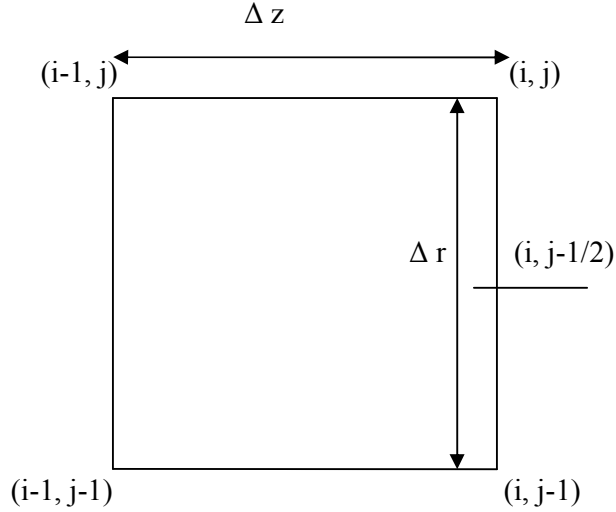
$$G_j = \left(\frac{v_{i-1, j}}{2\Delta r} \right) - \left(\frac{1}{\text{RePr}\Delta r^2} \right) - \left(\frac{1}{2r\Delta r} \right)$$

$$H_j = \left(\frac{u_{i-1, j}}{\Delta z} \right) (T_{i-1, j})$$

Similarly now we can apply the Thomas algorithm for momentum equation.

4.1.3 Implicit solution of continuity boundary layer equation

In order to express the non-dimensionalized governing equation (Continuity equation) using implicit scheme we follow the procedure:



Continuity equation has following derivatives.

$$\frac{\partial v}{\partial r} (i, j - 1/2) = \frac{u_{i, j+1} - u_{i, j-1}}{2\Delta r}$$

$$\frac{\partial u}{\partial z} (i, j - 1/2) = \frac{1}{2} \left[\frac{\partial u}{\partial z} (i, j) + \frac{\partial u}{\partial z} (i, j - 1) \right]$$

Using these derivatives in continuity equation

$$r \frac{\partial u}{\partial z} + \frac{\partial}{\partial r} (rv) = 0$$

Finally the continuity equation become in the following form from where we can easily find out v velocity.

$$[r v](i, j) = [r v](i, j - 1) - \Delta r \frac{r}{2} \left[\left(\frac{u_{i, j} - u_{i-1, j}}{\Delta z} \right) + \left(\frac{u_{i, j-1} - u_{i-1, j-1}}{\Delta z} \right) \right] \quad (26)$$

Now we use a FORTRAN 90 programming code in which will solve continuity equation simply and momentum equation as well as energy equation by using TDMA (Tridiagonal matrix solver algorithm). We solve continuity, momentum, energy equations simultaneously and to get values of temperature, u component as well as v component of velocity.

4.2 Numerical procedure of solving governing equation

The unsteady energy equation (5) is solved with the boundary conditions given in equation (6) to (8) and (10) using fourth order Runge-Kutta method (RK-4) for time integration and second order finite difference scheme for spatial derivatives. The solution started with the initial condition given in equation (11).

Here, $z_{\max} = 30$ with 1500 grid points distributed non-uniformly in the axial direction using the hyperbolic distribution given in equation (3). 100 points with equally divided in the radial direction is used. Very small time step $= 1 \times 10^{-6}$ taken to capture the fiber temperature accurately.

By using non-dimensionalized parameters explained in Chapter [2]; the governing non-dimensional energy equation in z, r plane is given by:

$$\frac{\partial \theta}{\partial t} = -\text{Pe} \frac{\partial \theta}{\partial z} + \left(\frac{\partial^2}{\partial r^2} + \frac{\partial^2}{\partial z^2} \right) \theta + \frac{1}{r} \frac{\partial \theta}{\partial r}$$

The Governing equation is transformed from (z, r) coordinates to (ξ, η) coordinates for higher resolution in the axial direction. The transformation from (z, r) to (ξ, η) is given by:

$$\frac{\partial \theta}{\partial t} = -\text{Pe} \frac{1}{h_1} \frac{\partial \theta}{\partial \xi} + \frac{1}{h_1} \left[\frac{\partial}{\partial \xi} \left(\frac{1}{h_1} \frac{\partial \theta}{\partial \xi} \right) + \frac{\partial}{\partial \eta} \left(h_1 \frac{\partial \theta}{\partial \eta} \right) \right] + \frac{1}{\eta} \frac{\partial \theta}{\partial \eta} \quad (27)$$

Where

$$\frac{\partial \theta}{\partial z} = \frac{1}{h_1} \frac{\partial \theta}{\partial \xi} = \frac{1}{h_1} \left[\frac{\theta_{i+1, j} - \theta_{i-1, j}}{2 \cdot \Delta \xi} \right]$$

$$\frac{\partial \theta}{\partial r} = \frac{\partial \theta}{\partial \eta} = \left[\frac{\theta_{i, j+1} - \theta_{i, j-1}}{2 \cdot \Delta \eta} \right]$$

$$\nabla^2 \theta = \left(\frac{\partial^2}{\partial r^2} + \frac{\partial^2}{\partial z^2} \right) \theta = \frac{1}{h_1} \left[\frac{\partial}{\partial \xi} \left(\frac{1}{h_1} \frac{\partial \theta}{\partial \xi} \right) + \frac{\partial}{\partial \eta} \left(h_1 \frac{\partial \theta}{\partial \eta} \right) \right]$$

Governing non-dimensionalization equation can be discretizing as:

$$\begin{aligned} \frac{\partial}{\partial \xi} \left(\frac{1}{h_1} \frac{\partial \theta}{\partial \xi} \right) &= \frac{\partial}{\partial \xi} \left[\left(\frac{1}{h_1} \right)_{i,j} \left(\frac{\theta_{i+1/2} - \theta_{i-1/2}}{\Delta \xi} \right) \right] \\ &= \frac{\partial}{\partial \xi} \left[\left(\frac{1}{h_1} \right)_{i,j} \left(\frac{\theta_{i+1/2}}{\Delta \xi} \right) \right] - \frac{\partial}{\partial \xi} \left[\left(\frac{1}{h_1} \right)_{i,j} \left(\frac{\theta_{i-1/2}}{\Delta \xi} \right) \right] \end{aligned} \quad (28)$$

Where

$$\frac{\partial}{\partial \xi} \left[\left(\frac{1}{h_1} \right)_{i,j} \left(\frac{\theta_{i+1/2}}{\Delta \xi} \right) \right] = \frac{1}{\Delta \xi} \left[\frac{\left(\frac{1}{h_1} \right)_{i+1/2,j} \theta_{i+1,j} - \left(\frac{1}{h_1} \right)_{i-1/2,j} \theta_{i,j}}{\Delta \xi} \right] \quad (29)$$

$$\frac{\partial}{\partial \xi} \left[\left(\frac{1}{h_1} \right)_{i,j} \left(\frac{\theta_{i-1/2}}{\Delta \xi} \right) \right] = \frac{1}{\Delta \xi} \left[\frac{\left(\frac{1}{h_1} \right)_{i+1/2,j} \theta_{i,j} - \left(\frac{1}{h_1} \right)_{i-1/2,j} \theta_{i-1,j}}{\Delta \xi} \right] \quad (30)$$

Therefore

$$\begin{aligned} &\frac{\partial}{\partial \xi} \left[\left(\frac{1}{h_1} \right)_{i,j} \left(\frac{\theta_{i+1/2}}{\Delta \xi} \right) \right] - \frac{\partial}{\partial \xi} \left[\left(\frac{1}{h_1} \right)_{i,j} \left(\frac{\theta_{i-1/2}}{\Delta \xi} \right) \right] \\ &= \frac{1}{\Delta \xi^2} \left[\left(\frac{1}{h_1} \right)_{i+1/2,j} \theta_{i+1,j} - \left\{ \left(\frac{1}{h_1} \right)_{i+1/2,j} + \left(\frac{1}{h_1} \right)_{i-1/2,j} \right\} \theta_{i,j} + \left(\frac{1}{h_1} \right)_{i-1/2,j} \theta_{i-1,j} \right] \end{aligned}$$

But we know

$$\left(\frac{1}{h_1} \right)_{i+1/2,j} = \left[\frac{\left(\frac{1}{h_1} \right)_i + \left(\frac{1}{h_1} \right)_{i+1}}{2} \right] \quad (31)$$

$$\left(\frac{1}{h_1}\right)_{i-1/2, j} = \left[\frac{\left(\frac{1}{h_1}\right)_i + \left(\frac{1}{h_1}\right)_{i-1}}{2} \right] \quad (32)$$

Finally the discretized term:

$$\begin{aligned} & \frac{\partial}{\partial \xi} \left(\frac{1}{h_1} \frac{\partial \theta}{\partial \xi} \right) \\ &= \frac{1}{\Delta \xi^2} \left[\left\{ \frac{\left(\frac{1}{h_1}\right)_i + \left(\frac{1}{h_1}\right)_{i+1}}{2} \right\} \theta_{i+1, j} - \left\{ \frac{\left(\frac{1}{h_1}\right)_{i+1} + 2\left(\frac{1}{h_1}\right)_i + \left(\frac{1}{h_1}\right)_{i-1}}{2} \right\} \theta_{i, j} \right. \\ & \quad \left. + \left\{ \frac{\left(\frac{1}{h_1}\right)_i + \left(\frac{1}{h_1}\right)_{i-1}}{2} \right\} \theta_{i-1, j} \right] \end{aligned}$$

And

$$\frac{\partial}{\partial \eta} \left(h_1 \frac{\partial \theta}{\partial \eta} \right) = (h_1)_{i, j} \frac{1}{\Delta \eta^2} [\theta_{i, j+1} - 2\theta_{i, j} + \theta_{i, j-1}]$$

$$\begin{aligned} & \frac{1}{h_1} \left[\frac{\partial}{\partial \xi} \left(\frac{1}{h_1} \frac{\partial \theta}{\partial \xi} \right) + \frac{\partial}{\partial \eta} \left(h_1 \frac{\partial \theta}{\partial \eta} \right) \right] \\ &= \frac{1}{h_1} \frac{1}{\Delta \xi^2} \left[\left\{ \frac{\left(\frac{1}{h_1}\right)_i + \left(\frac{1}{h_1}\right)_{i+1}}{2} \right\} \theta_{i+1, j} - \left\{ \frac{\left(\frac{1}{h_1}\right)_{i+1} + 2\left(\frac{1}{h_1}\right)_i + \left(\frac{1}{h_1}\right)_{i-1}}{2} \right\} \theta_{i, j} \right. \\ & \quad \left. + \left\{ \frac{\left(\frac{1}{h_1}\right)_i + \left(\frac{1}{h_1}\right)_{i-1}}{2} \right\} \theta_{i-1, j} \right] + \frac{1}{h_1} \frac{1}{\Delta \eta^2} [(h_1)_{i, j} (\theta_{i, j+1} - 2\theta_{i, j} + \theta_{i, j-1})] \end{aligned} \quad (33)$$

Putting all terms in the equation (27);

$$\begin{aligned}
& \frac{\partial \theta}{\partial t} \\
& = -\text{Pe} \frac{1}{h_1} \left(\frac{\theta_{i+1, j} - \theta_{i-1, j}}{2\Delta\xi} \right) \\
& + \frac{1}{h_1} \frac{1}{\Delta\xi^2} \left[\left\{ \frac{\left(\frac{1}{h_1}\right)_i + \left(\frac{1}{h_1}\right)_{i+1}}{2} \right\} \theta_{i+1, j} - \left\{ \frac{\left(\frac{1}{h_1}\right)_{i+1} + 2\left(\frac{1}{h_1}\right)_i + \left(\frac{1}{h_1}\right)_{i-1}}{2} \right\} \theta_{i, j} \right. \\
& \left. + \left\{ \frac{\left(\frac{1}{h_1}\right)_i + \left(\frac{1}{h_1}\right)_{i-1}}{2} \right\} \theta_{i-1, j} \right] + \frac{1}{h_1} \frac{1}{\Delta\eta^2} [(h_1)_{i, j} (\theta_{i, j+1} - 2\theta_{i, j} + \theta_{i, j-1})] \\
& + \frac{1}{\eta} \left(\frac{\theta_{i, j+1} - \theta_{i, j-1}}{2\Delta\eta} \right)
\end{aligned}$$

Finally governing equation:

$$\begin{aligned}
& \frac{\partial \theta}{\partial t} \\
& = -\text{Pe} \frac{1}{h_1} \left(\frac{\theta_{i+1, j} - \theta_{i-1, j}}{2\Delta\xi} \right) \\
& + \frac{1}{h_1} \frac{1}{\Delta\xi^2} \left[\left\{ \frac{\left(\frac{1}{h_1}\right)_i + \left(\frac{1}{h_1}\right)_{i+1}}{2} \right\} \theta_{i+1, j} - \left\{ \frac{\left(\frac{1}{h_1}\right)_{i+1} + 2\left(\frac{1}{h_1}\right)_i + \left(\frac{1}{h_1}\right)_{i-1}}{2} \right\} \theta_{i, j} \right. \\
& \left. + \left\{ \frac{\left(\frac{1}{h_1}\right)_i + \left(\frac{1}{h_1}\right)_{i-1}}{2} \right\} \theta_{i-1, j} \right] + \frac{1}{\Delta\eta^2} (\theta_{i, j+1} - 2\theta_{i, j} + \theta_{i, j-1}) + \frac{1}{\eta} \left(\frac{\theta_{i, j+1} - \theta_{i, j-1}}{2\Delta\eta} \right)
\end{aligned} \tag{34}$$

We use fourth order Runge-Kutta method to get the surface temperature, center temperature and contour profiles. This method is fourth-order accurate. Consider the solution of our equation is of following type:

$$\theta_{i+1} = \theta_i + \frac{1}{6} [K_1 + 2.K_2 + 2.K_3 + K_4] \tag{35}$$

Where θ_i is a function of (z_i, r_i) .

$$K_1 = \Delta t \times \theta_i(z_i, r_i)$$

$$K_2 = \Delta t \times \theta_i(z_i, r_i) + \frac{K_1}{2}$$

$$K_3 = \Delta t \times \theta_1(z_i, r_i) + \frac{K_2}{2}$$

$$K_4 = \Delta t \times \theta_1(z_i, r_i) + K_3$$

Now we use a FORTRAN 90 programming code to solve governing energy equation by using fourth order Runge-Kutta method to get temperature profiles.

We have solved the equations double precision accuracy to avoid round off error. We have used second order accuracy to reduce the truncation error. We have used very small time step to avoid numerical instability.

Chapter 5

Results and discussion

In this chapter numerical results are given for the cooling of optical fibers. Prior to that, descriptions of the geometry, the boundary conditions and other relevant aspects implemented in numerical code are briefly highlighted.

An optical fiber during the cooling stage of the drawing process was modeled as an infinite cylinder moving in still air at a constant speed. Axial as well as the radial temperature distributions during the cooling process is considered. To perform a thermal analysis of the process, the heat transfer modes that take place during the drawing of fibers, an unsteady state governing energy equation and laminar boundary layer formation are considered.

5.1 Convection results

The steady boundary layer equations (15) to (17) of air around the fiber are solved using implicit finite difference method as given in section 4.1 to find the temperature profiles. The average convective heat transfer coefficient is obtained using the equation (23) from the boundary layer solution and it is used in equation (35) to get surface temperature of the fiber during cooling stage. Convective heat transfer values are obtained and tabulated in Table 5.1 for different speed and size of the optical fiber.

Here, $z_{\max} = 15$ with 1500 grid points distributed non-uniformly in the axial direction and $R_{\max} = 4.5$ with 300 points equally divided in the radial direction is used. A constant Prandtl number ($Pr = 0.7$) was used for air.

Table 5.1: BK7 material cases

Material	Fiber Type	U	D	Re	Nu_{avg}	Convective heat transfer coefficient (w/m²k)
BK7	Thick	1.0 cm/s	0.5 mm	0.0861	0.2727	26.6696
BK7	Thick	1.0 cm/s	1.0 mm	0.1723	0.2983	14.5859
BK7	Thick	1.0 cm/s	1.5 mm	0.2584	0.3257	10.6169
BK7	Thick	2.9 cm/s	1.0 mm	0.5	0.4130	20.1921
BK7	Thick	5.8 cm/s	1.0 mm	1.0	0.6471	31.6364
BK7	Thick	8.7 cm/s	1.0 mm	1.5	0.9595	46.9114
BK7	Thick	11.6 cm/s	1.0 mm	2.0	1.3508	66.0416

First results are obtained for the case of $Re = 0.0861$ which corresponds the speed and diameter of the fiber are 1.0 cm/s and 0.5 mm. The temperature and axial velocity contours are shown in Figures 5.1 and 5.2 for the case of $Re = 0.0861$. The average Nusselt number value $Nu_{avg} = 0.2727$ using the equation (23) for $Re = 0.0861$. The corresponding convective heat transfer coefficient is $h = 26.6696 \text{ W/m}^2\text{K}$. From Figure 5.1 the temperature contours shows the formation of thermal boundary layer around the fiber and the temperature values are decreasing with the increase of distance from the surface. From Figure 5.2 the u velocity contours shows the formation of thermal boundary layer around the fiber and the values of u velocity contours are decreasing with the increase of distance from the surface.

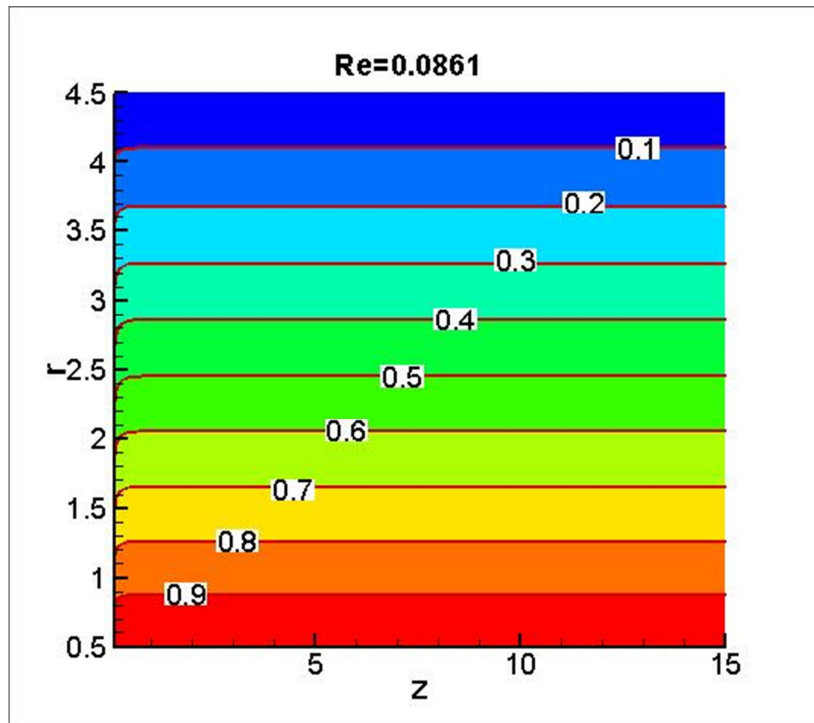


Figure 5.2: Temperature contours for $Re = 0.0861$

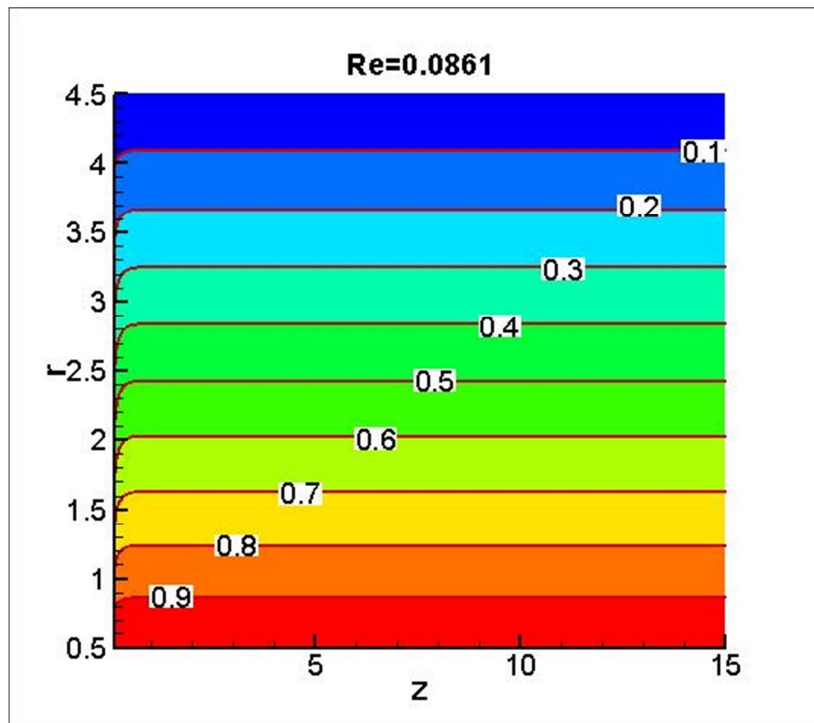


Figure 5.2: Axial velocity contours for $Re = 0.0861$

As the diameter increases from 0.5 mm to 1.0 mm with a constant speed of the fiber corresponding $Re = 0.1723$. The temperature and axial velocity contours are shown in Figures 5.3 and 5.4 for the case of $Re = 0.1723$. From Figure 5.3 the temperature contours shows the formation of thermal boundary layer around the fiber and the temperature values are decreasing with the increase of distance from the surface. From Figure 5.4 the u velocity contours shows the formation of thermal boundary layer around the fiber and the values of u velocity contours are decreasing with the increase of distance from the surface. The average Nusselt number value $Nu_{avg} = 0.2983$ using the equation (23) for $Re = 0.1723$. The corresponding convective heat transfer coefficient is $h = 14.5859 \text{ W/m}^2 \text{ K}$. Convective heat transfer (h) value decreases with the increases of diameter at a constant speed because the surface area increases.

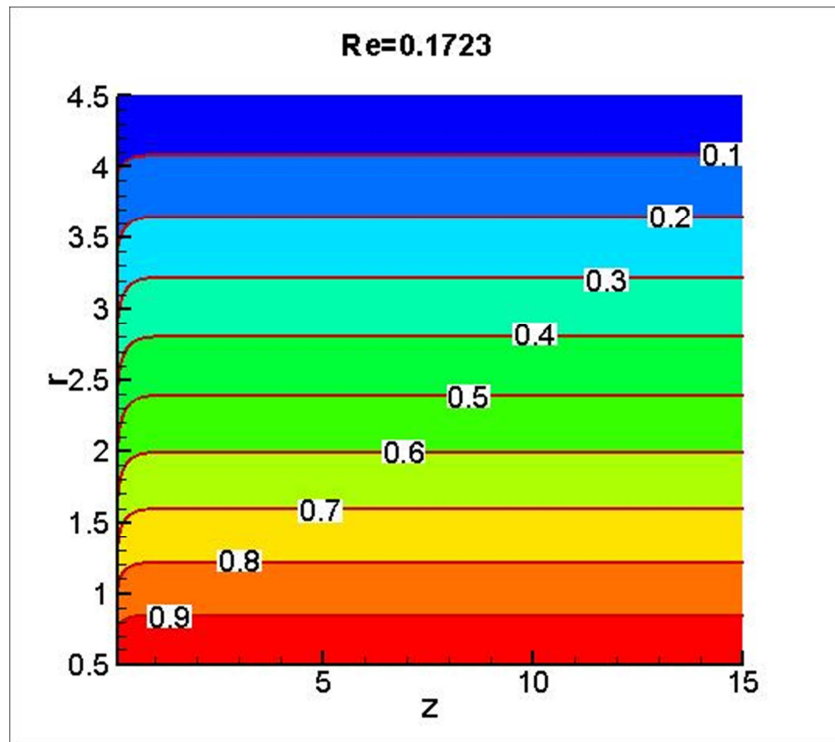


Figure 5.3: Temperature contours for $Re = 0.1723$

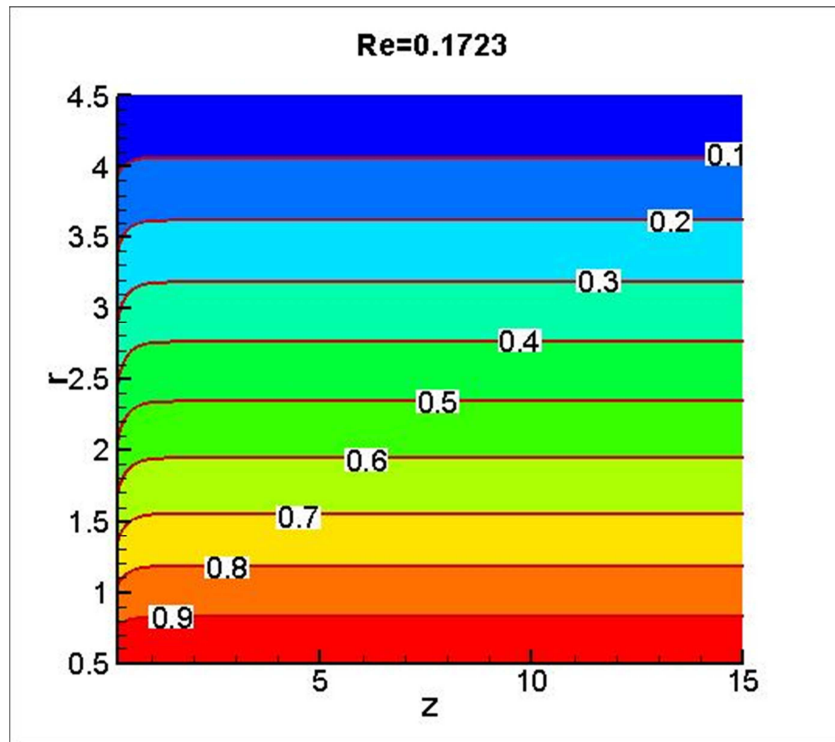


Figure 5.4: Axial velocity contours for $Re = 0.1723$

As the diameter increases from 1.0 mm to 1.5 mm with a constant speed of the fiber corresponding $Re = 0.2584$. The temperature and axial velocity contours are shown in Figures 5.5 and 5.6 for the case of $Re = 0.2584$. From Figure 5.5 the temperature contours shows the formation of thermal boundary layer around the fiber and the temperature values are decreasing with the increase of distance from the surface.

From Figure 5.6 the u velocity contours shows the formation of thermal boundary layer around the fiber and the values of u velocity contours are decreasing with the increase of distance from the surface. The average Nusselt number value $Nu_{avg} = 0.3257$ using the equation (23) for $Re = 0.2584$. The corresponding convective heat transfer coefficient is $h = 10.6169 \text{ W/m}^2 \text{ K}$. Convective heat transfer (h) value decreases with the increases of diameter at a constant speed because the surface area increases.

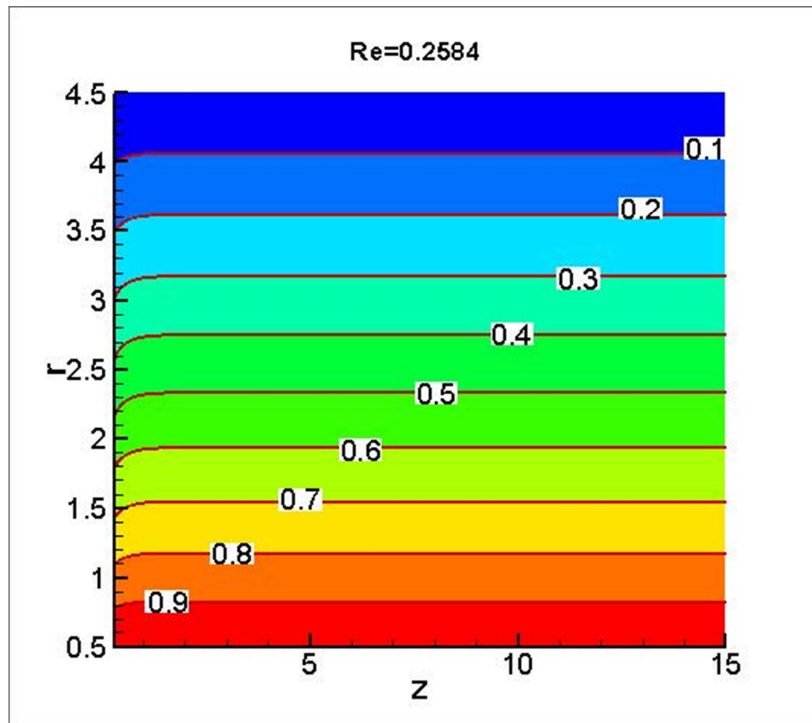


Figure 5.5: Temperature contours for $Re = 0.2584$

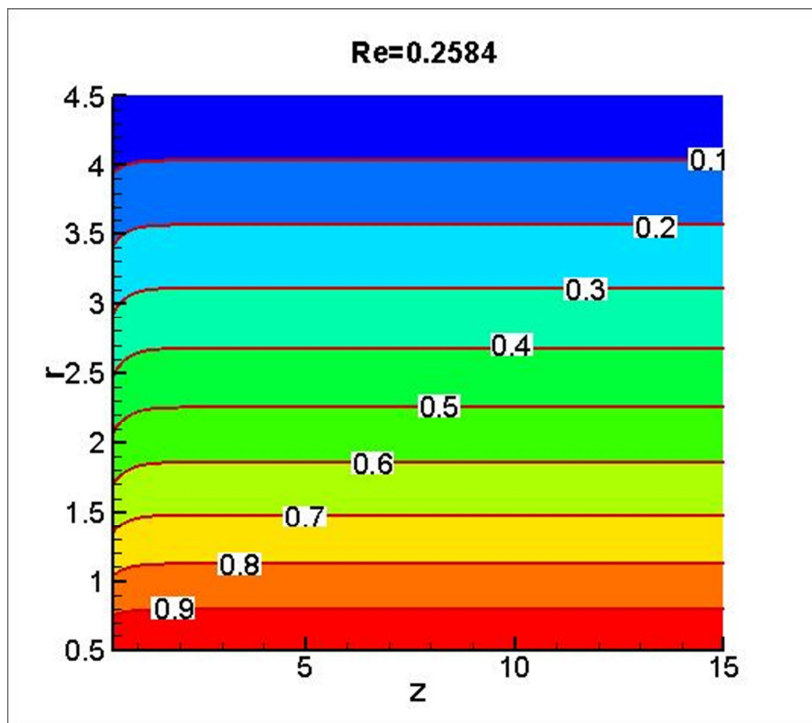


Figure 5.6: Axial velocity contours for $Re = 0.2584$

At the diameter 1.0 mm with a constant speed of the fiber 2.9014 corresponding $Re = 0.1723$. As the speed of the fiber increases from 2.9014 cm/s to 5.8029 cm/s with a constant diameter of the fiber corresponding $Re = 1.0$. Similarly As the speed of the fiber increases from 5.8029 cm/s to 8.7043 cm/s with a constant diameter of the fiber corresponding $Re = 1.5$ and as the speed of the fiber increases from 8.7043 cm/s to 11.6058 cm/s with a constant diameter of the fiber corresponding $Re = 2.0$.

The temperature and axial velocity contours are shown in Figures 5.7 and 5.8 together for all cases of $Re = 0.5, 1.0, 1.5$ and 2.0 .

From Figure 5.7 the temperature contours shows the formation of thermal boundary layer around the fiber and the temperature values are decreasing with the increase of distance from the surface as Re number increases.

From Figure 5.8 the u velocity contours shows the formation of thermal boundary layer around the fiber and the values of u velocity contours are decreasing with the increase of distance from the surface as Re number increases. The average Nusselt number and convective heat transfer values related to Re numbers are shown in the Table 5.1.

As the velocity increases with a fixed diameter of the fiber so the corresponding Re value increases with the increase of velocity of fiber. As Re increases, the convective heat transfer coefficient increases means it cools faster with the increasing speed of the fiber at a fixed diameter of the fiber.

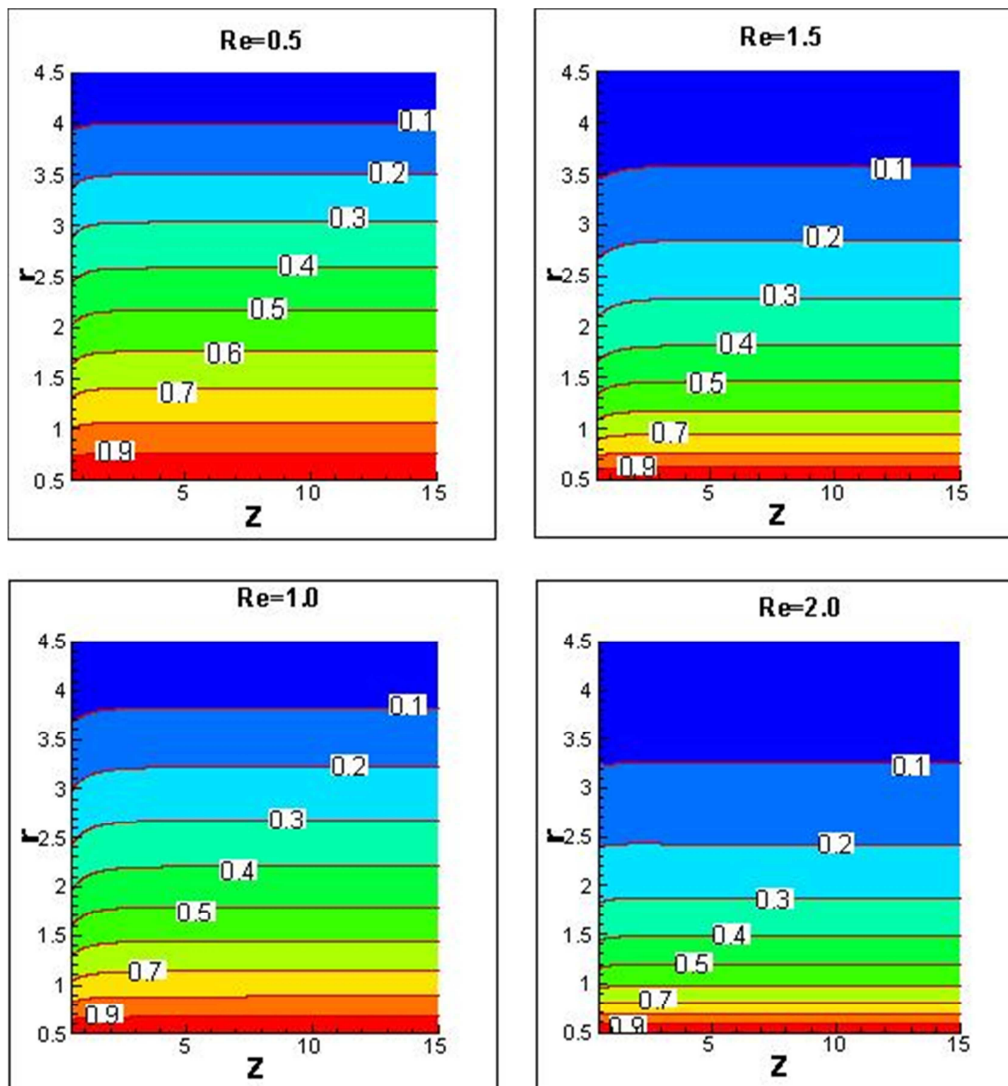


Figure 5.7: Temperature contours for Re = 0.5, 1.0, 1.5 and 2.0

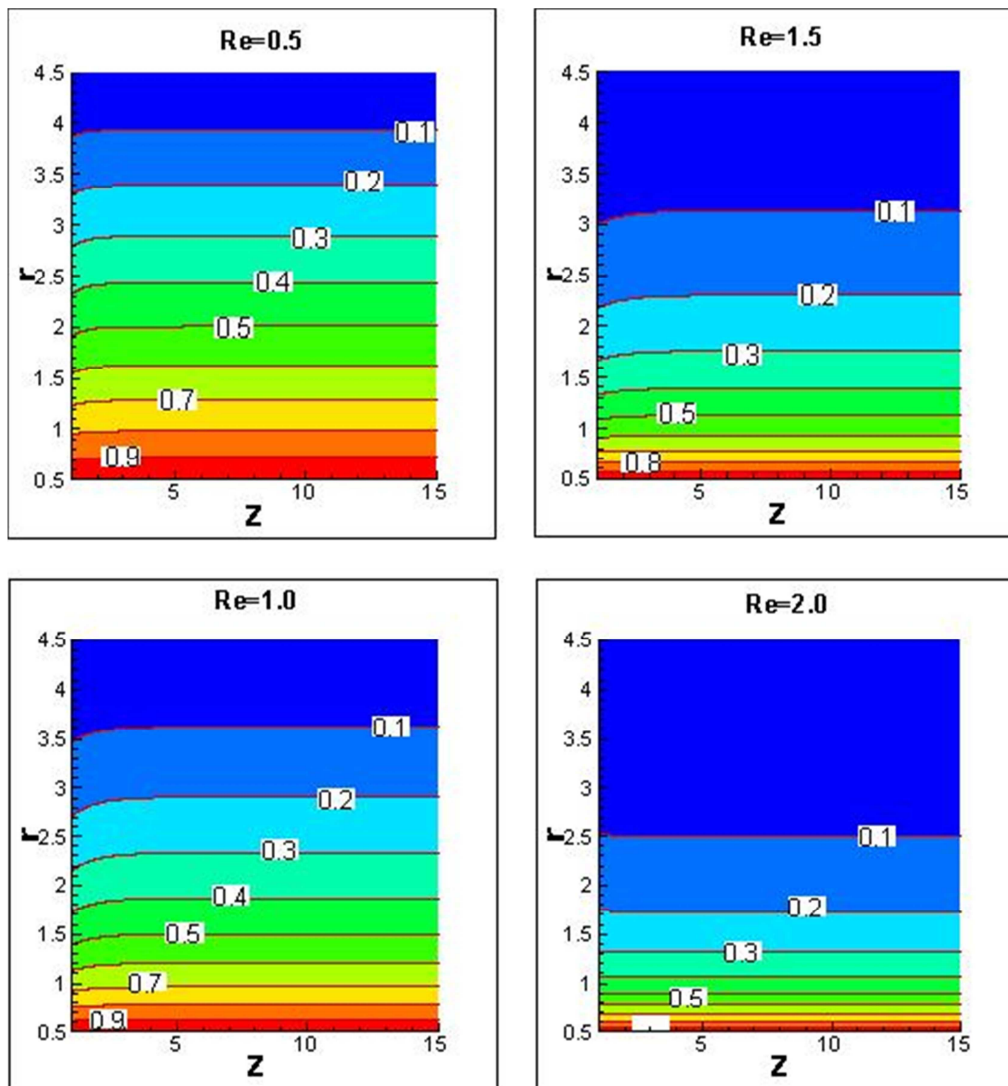


Figure 5.8: Axial velocity contours for Re = 0.5, 1.0, 1.5 and 2.0

For Validation of h value we can compare present results with Kase and Matsuto relation. Table 5.2, Shows the comparison of present cases with cases obtained by Kase and Matsuto relation who is already exists in Literature.

Kase and Matsuto provided the generally accepted correlation for a stationary thin cylinder parallel to the airflow:

$$\text{Correlation } Nu_a = \frac{hD}{k} = 0.42(Re_a)^{0.344} \quad (36)$$

Kase and Matsuto developed their correlation based on the data they obtained by subjecting a 0.2 mm diameter heated wire to airflow parallel to wire for values of Re_a in the range up to 50. Present results are shows the same trend of the correlation results reported in Kase and Matsuto [20]. Present results are high accuracy compared to the correlation results because the correlation is obtained based on few experiments only. They have not included the effect of Prandtl number.

Table 5.2: Validation of h value

Material	Fiber Type	U	D	Re	Present h value (w/m ² k)	Correlation h value (w/m ² k)
BK7	Thick	1.0 cm/s	0.5 mm	0.0861	26.6696	17.6651
BK7	Thick	1.0 cm/s	1.0 mm	0.1723	14.5859	11.2100
BK7	Thick	1.0 cm/s	1.5 mm	0.2584	10.6169	08.5912

Convective heat transfer (h) value decreases with the increases of diameter at a constant speed because the surface area increases.

5.2 Transient results

The unsteady energy equation (5) is solved using RK4 time integration scheme with central finite difference schemes for spatial derivatives and details given in section 4.2 to find the surface temperature of the fiber during the cooling stage of the drawing process. Here, $z_{max} = 30$ with 1500 grid points distributed non-uniformly in the axial direction using the hyperbolic distribution given in equation (3). 100 points with equally divided in the radial direction is used. Very small time step $t = 1 \times 10^{-6}$ taken to capture the fiber temperature accurately.

5.2.1 Validation of numerical approach

First to validate the numerical approach, the results are obtained for the case of $Pe = 0.2$ and $Bi = 5.0$ to compare previous results given in Roy choudhury and Jaluira [18]. They have reported transient temperature distribution of the moving rod using infinite series solution. The temperature contours are shown in Figures 5.10 and 5.12 at time $t = 3$ and $t = 10$ for $Pe = 0.2$ with $Bi = 5.0$. The temperature contours plotted in Figures 5.9 and 5.11 are obtained

with the length scale as R instead of D to compare the present results with reported results in Roy choudhury and Jaluria [18]. From Figures 5.10 and 5.12, the temperature contours shown the same trend and nature as reported in Roy Choudhury and Jaluria [18].

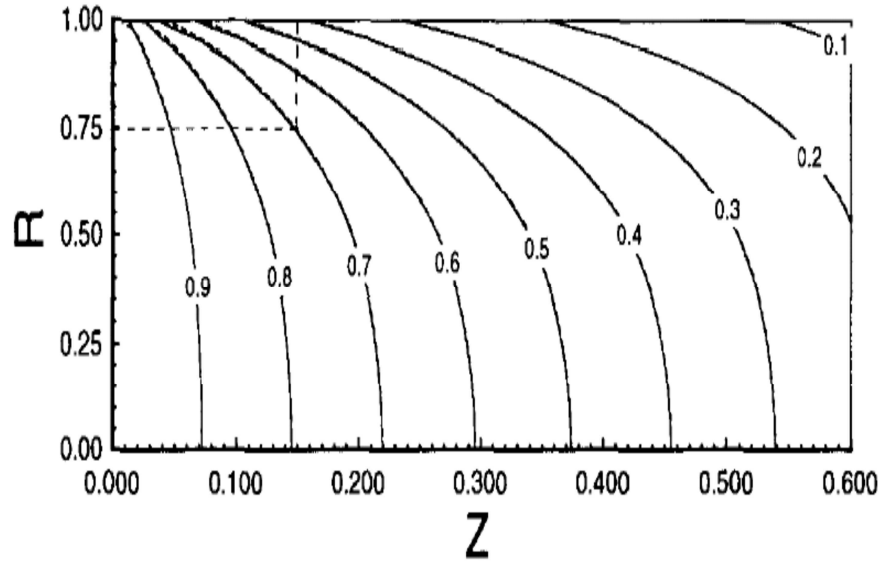


Figure 5.9: Temperature contours at $t = 3$ reported by Roy and Jaluria [18]

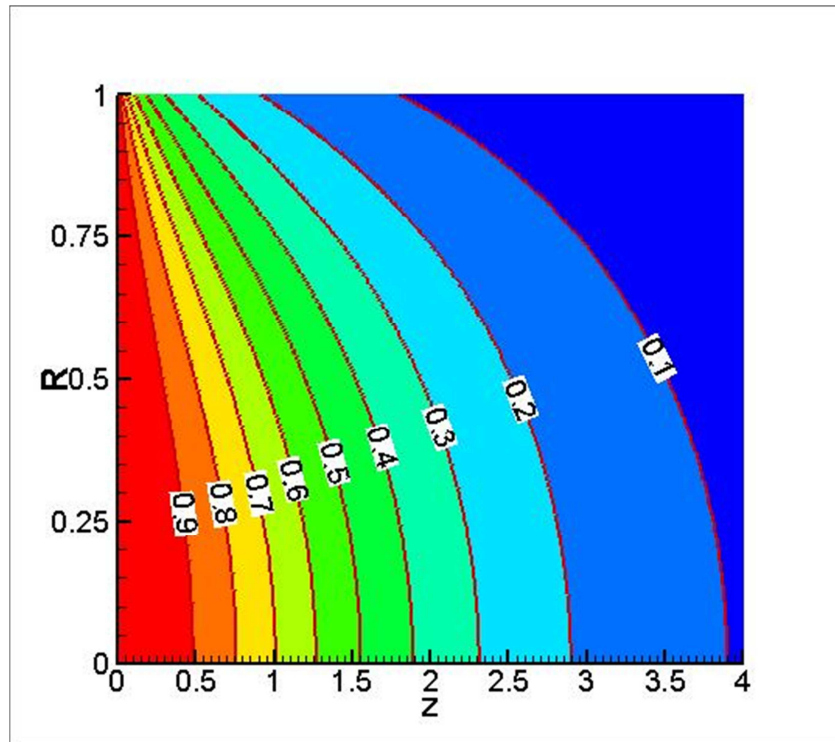


Figure 5.10: Temperature contours $t=3$

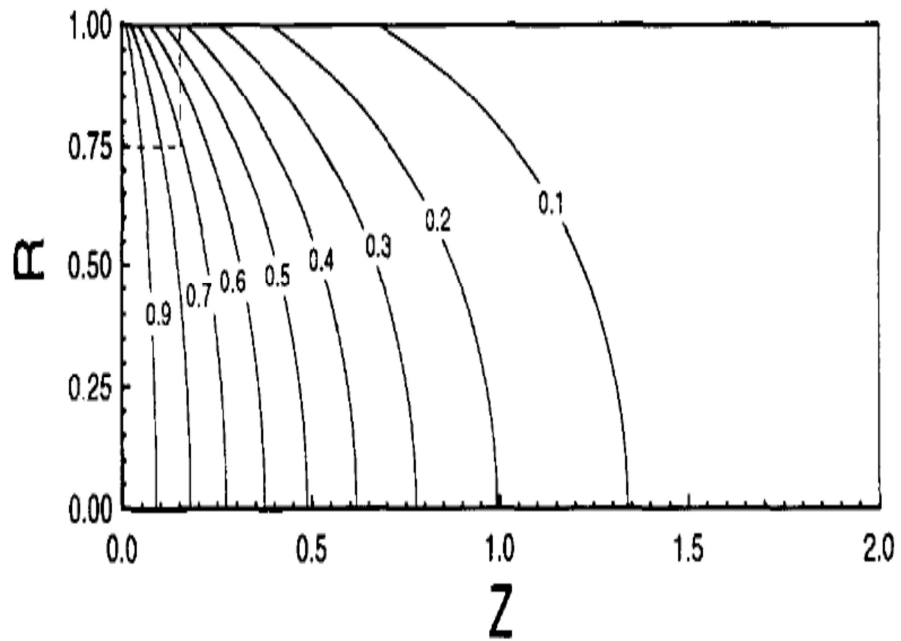


Figure 5.11: Temperature contours at $t = 10$ reported by Roy and Jaluria [18]

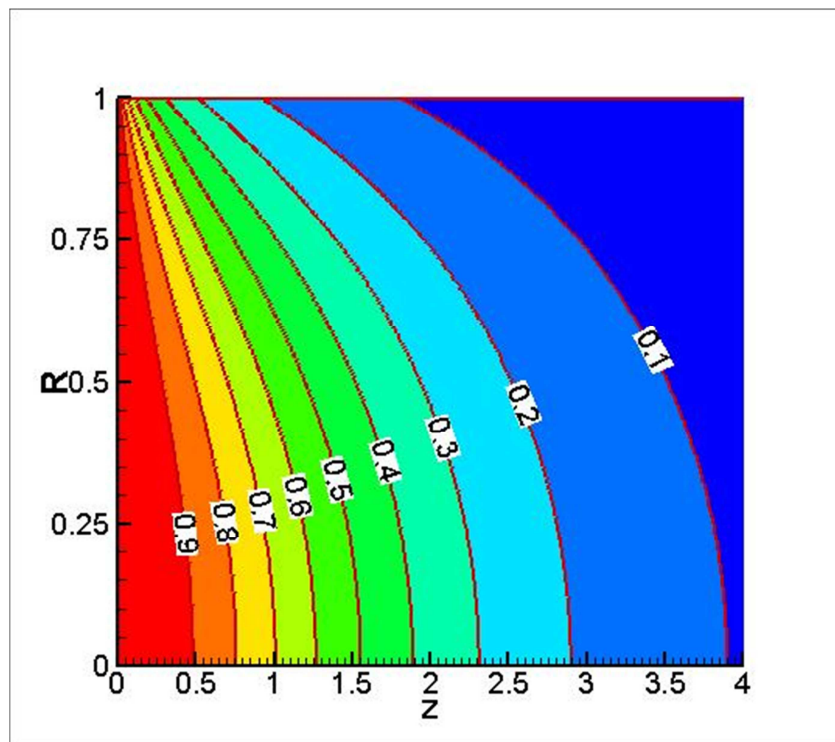


Figure 5.12: Temperature contours at $t = 10$

The surface and center temperature are shown in Figures 5.14 and 5.16 at time $t = 3$ and $t = 10$ for $Pe = 0.2$ with $Bi = 5$. From Figures 5.13 and 5.15, the surface and center temperature profiles are exactly matches with results given in Roy Choudhury and Jaluria [18].

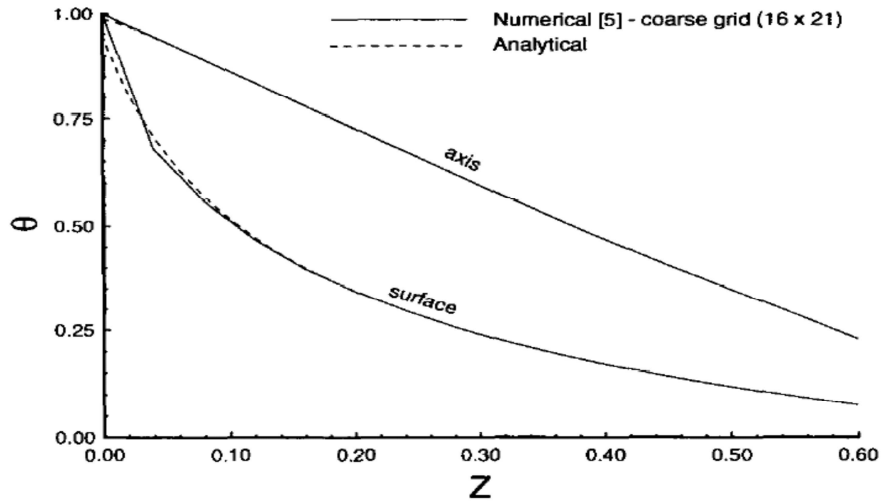


Figure 5.13: Surface & center temperatures at $t = 3$ reported by Roy and Jaluria [18]

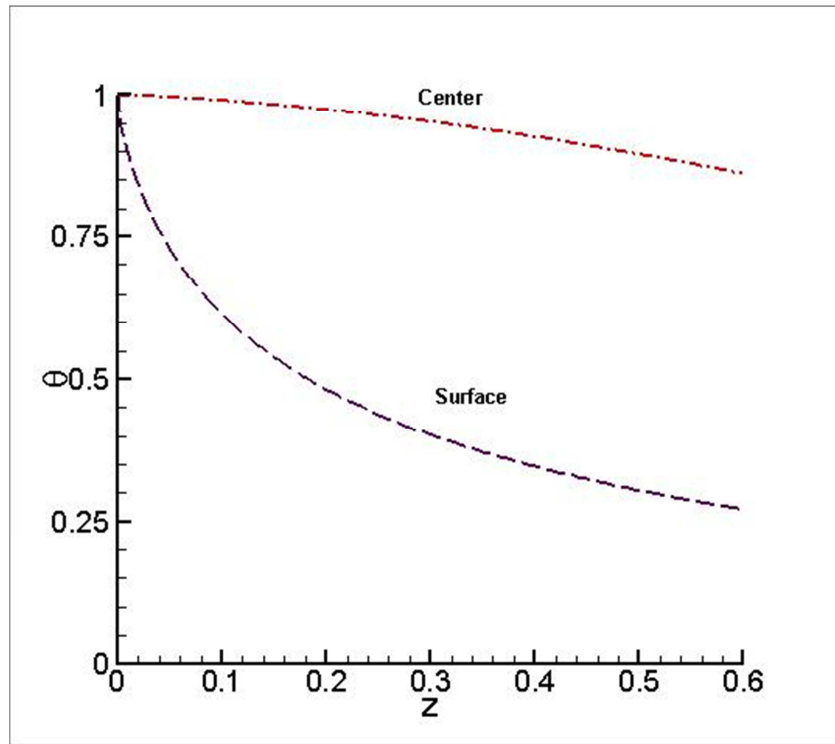


Figure 5.14: Surface & center temperatures at $t = 3$

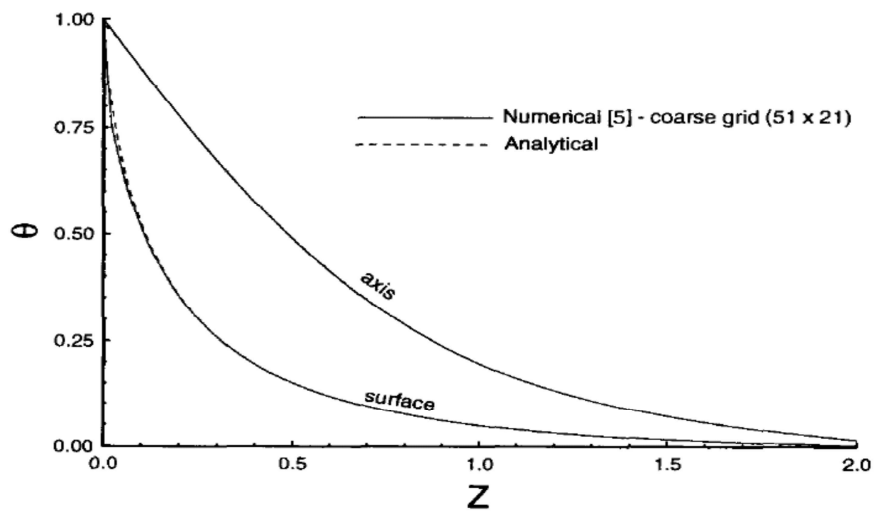


Figure 5.15: Surface & center temperatures at $t=10$ reported by Roy and Jaluria [18]

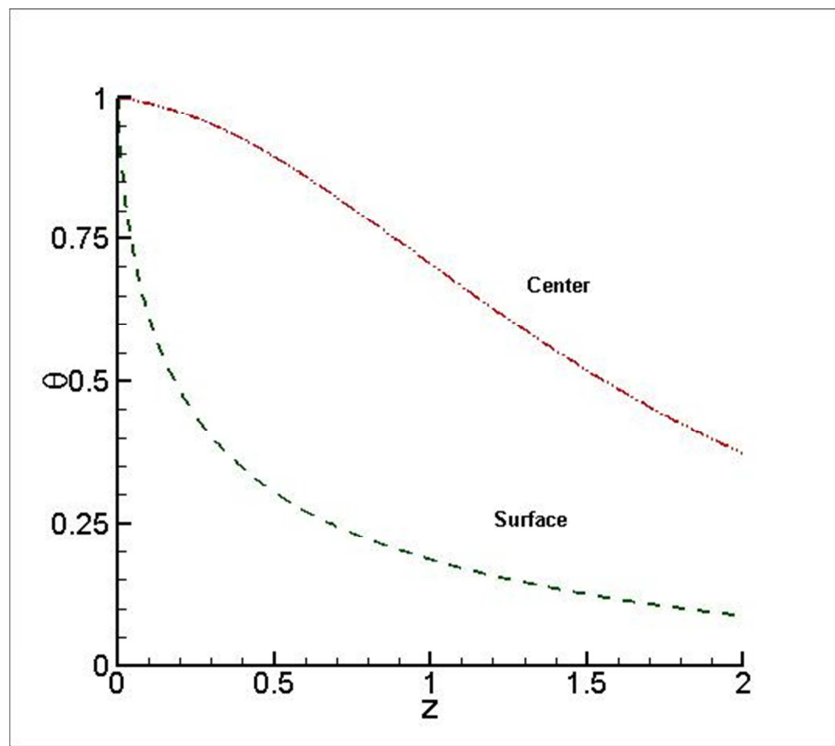


Figure 5.16: Surface & center temperatures at $t = 10$

Present results are high accuracy compared to Roy Choudhury and Jaluria [18] because they have reported analytical solution with infinite series solution method.

5.2.2 Selection of Z_{\max}

The diameter and drawing speed of the BK7 optical fiber are 1.0 mm and 1.0 cm/s corresponding dimensionless numbers are $Pe = 19.33226$ and $Bi = 0.02278$. The temperature of the fiber at the exit of the furnace is chosen in the range of 700C to 1000 C. The surface temperature show in Figure 5.17 with different Z_{\max} values at time $t = 5$ and $t = 13$ for $Pe = 19.33226$ and $Bi = 0.02278$. From Figure 5.17, one can notice that as time progress the cooling rate is faster and the surface temperature is not changing much with increasing Z_{\max} from $Z_{\max} = 30$ to 50. Hence, all cases are reported with maximum axial distance $Z_{\max} = 30$.

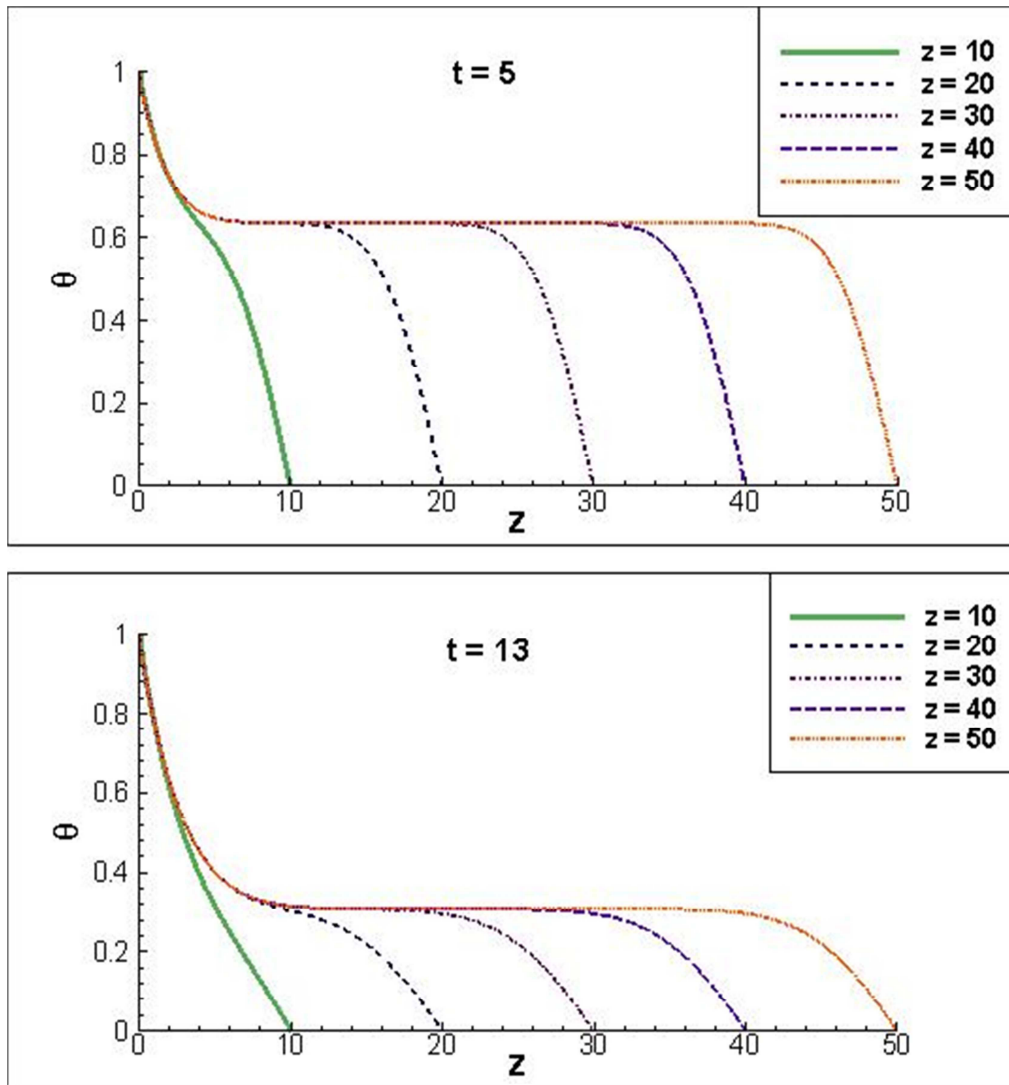


Figure 5.37: Surface temperatures at $Z_{\max} = 10, 20, 30, 40, 50$

The cooling rate of the optical fiber during the cooling stage of drawing process are obtained with varying velocity , diameter and material and all the cases considered here are tabulated in Table 5.3.

Table 5.3: Effect of drawing speed and size of the optical fiber

Material	Drawing Velocity	Diameter	Pe	h Value (w/m²k)	Bi
BK7	1.0 cm/s	0.5 mm	9.6661	26.6696	0.0119
BK7	1.0 cm/s	1.0 mm	19.3322	14.5859	0.0130
BK7	1.0 cm/s	1.5 mm	28.9983	10.6169	0.0142
BK7	0.5 cm/s	1.0 mm	9.6661	13.3348	0.0119
BK7	1.5 cm/s	1.0 mm	28.9983	15.9254	0.0142
BK7	1.0 m/s	1.0 mm	1933.2264	922.0173	0.8276
BK7	1.0 m/s	3.0 mm	5799.6791	772.2728	2.0797
VYCOR	1.0 cm/s	0.5 mm	5.9239	26.6696	0.0096
VYCOR	1.0 cm/s	1.0 mm	11.8478	14.5859	0.0105
VYCOR	1.0 cm/s	1.5 mm	17.7717	10.6169	0.0115
VYCOR	0.5 cm/s	1.0 mm	5.9239	13.3348	0.0096
VYCOR	1.5 cm/s	1.0 mm	17.7717	15.9254	0.0115

The diameter and drawing speed of the BK7 optical fiber are 1.0 mm and 1.0 cm/s corresponding dimensionless numbers are $Pe = 19.3322$ and $Bi = 0.0130$ as given in Table 5.3. The average convective heat transfer coefficient is obtained from the boundary layer solution as discussed in previous section 4.1. The temperature contours are shown in Figure 5.18 with different times $t = 5, 10, 20$ and 30 for the case of $Pe = 19.3322$ with $Bi = 0.0130$. The surface and center temperatures with different times for the case of $Pe = 19.3322$ and $Bi = 0.0130$ as shown in Figures 5.19 and 5.20. From Figures 5.18, 5.19 and 5.20, one can notice that , the temperature values decreases with the increase of time means optical fiber cools as the time progress. The fiber temperature values are not changing much after $t = 30$. So steady state temperature of fiber is at $t = 30$.

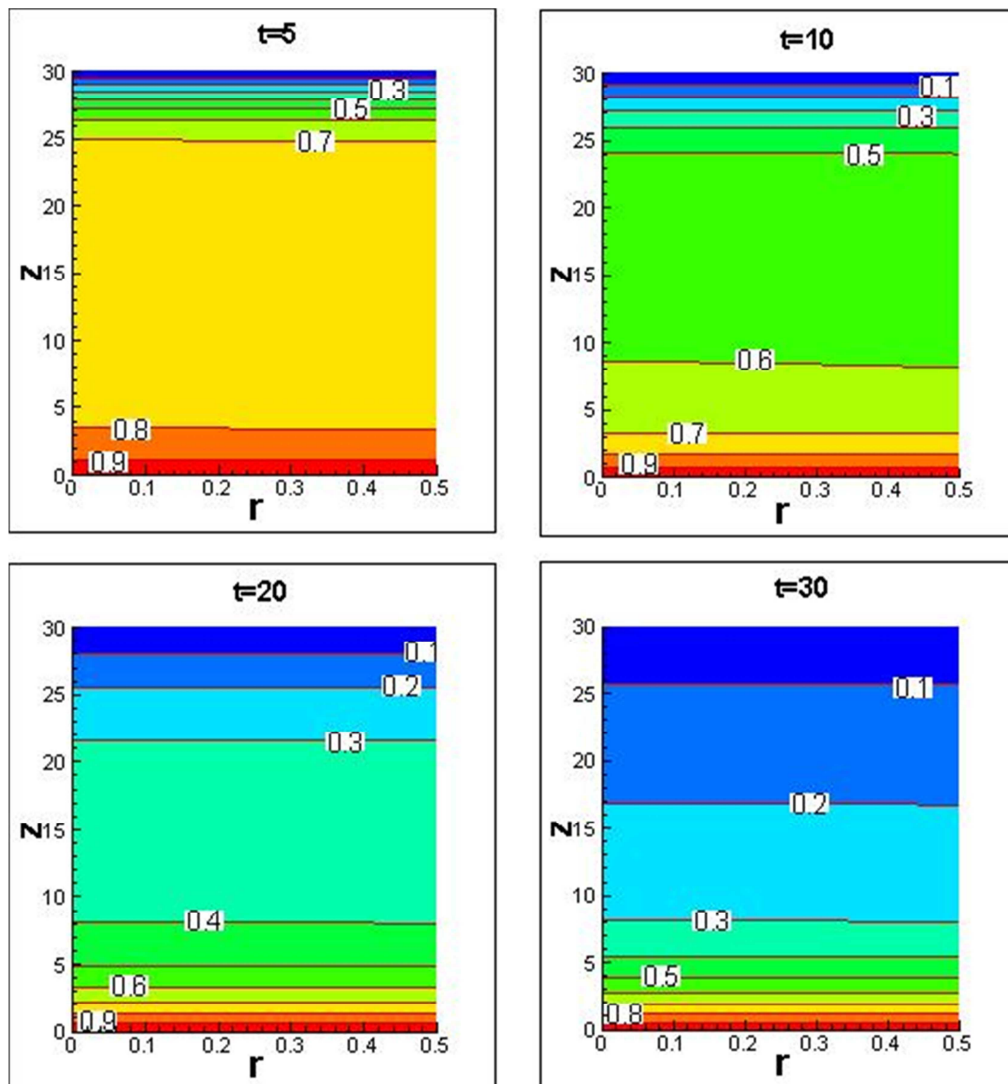


Figure 5.18: Temperature contours at $t = 5, 10, 20$ and 30

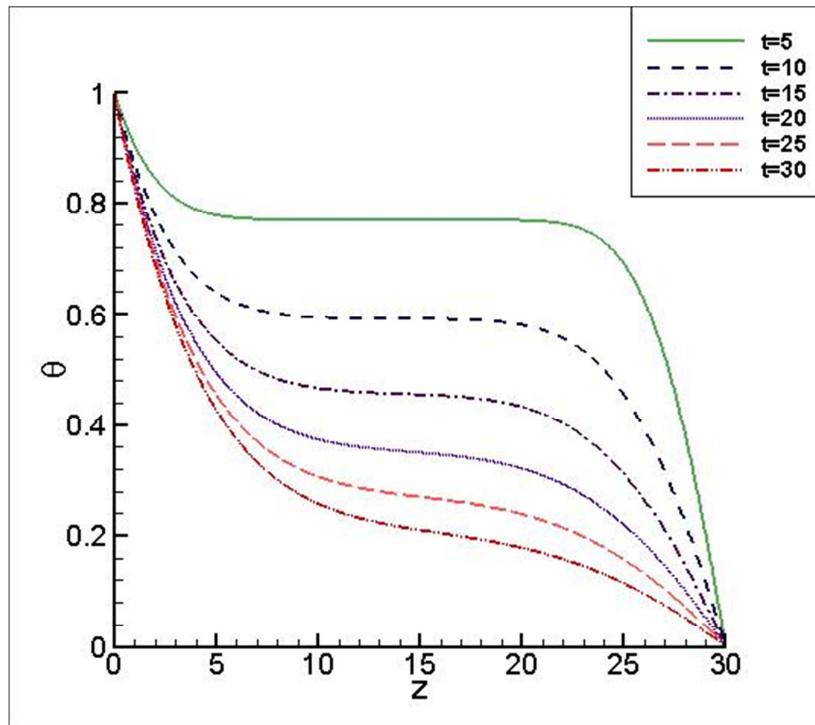


Figure 5.19: Surface temperature at different time

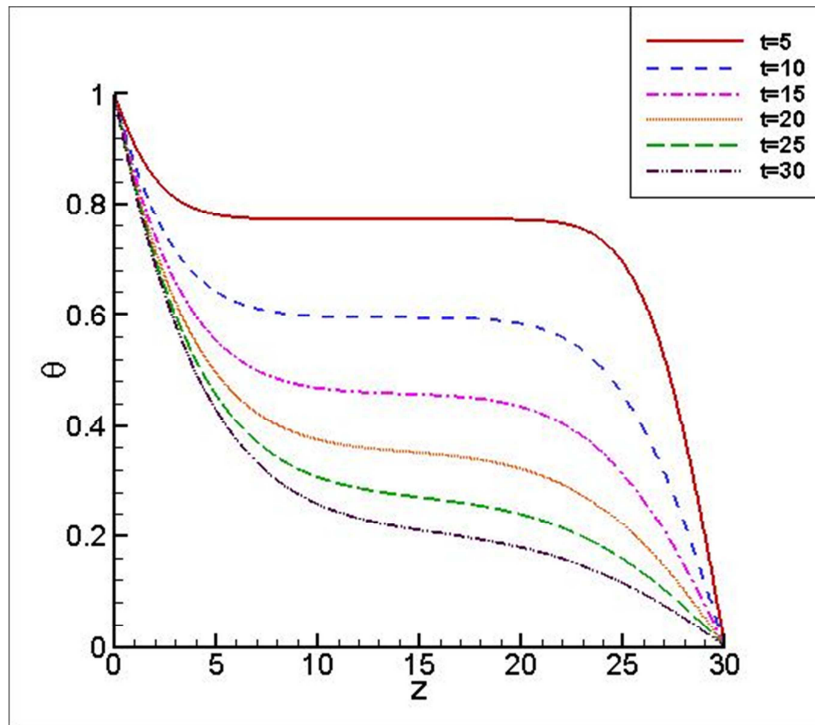


Figure 5.20: Center temperature at different time

The temperature contours are shown in Figures 5.21 and 5.22 for $Pe = 28.9983$, $Bi = 0.0142$. Surface and Center temperatures are shown in Figures 5.23 and 5.24 for $Pe = 28.9983$, $Bi = 0.0142$. For $Pe = 28.9983$ and $Bi = 0.0142$ the corresponding possible combinations of physical parameters are given by:

- Drawing velocity $U = 1.0$ cm/s and Diameter of fiber $D = 1.5$ mm.
- Drawing velocity $U = 1.5$ cm/s and diameter of fiber $D = 1.0$ mm

From Figures 5.21, 5.22, 5.23 and 5.24, one can notice that the temperature values decreases with the increase of time means optical fiber cools as the time progress. The fiber temperature values are not changing much after $t = 30$. So steady state temperature of fiber is at $t = 30$.

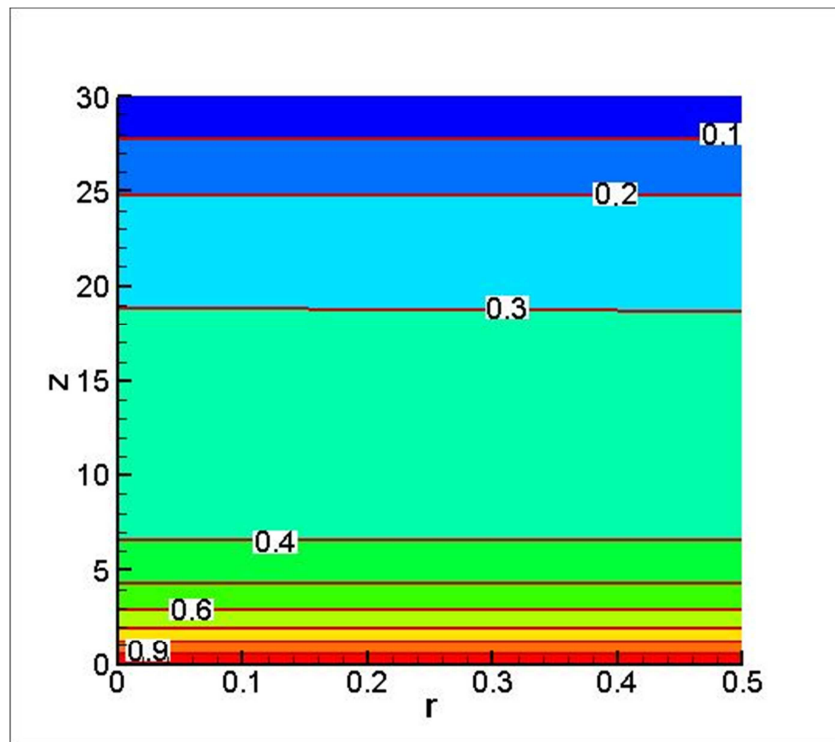


Figure 5.21: Temperature contours at $t = 20$

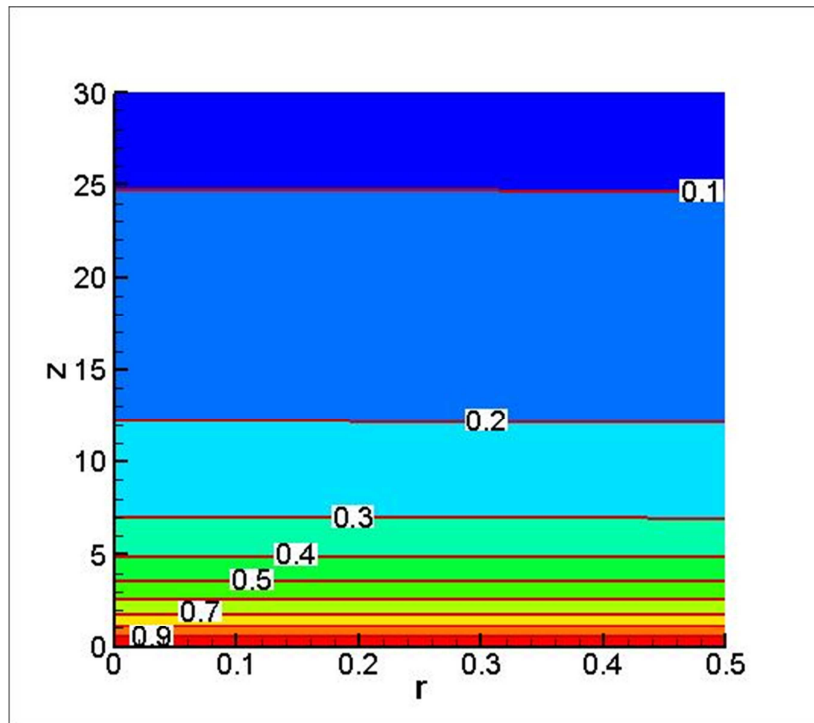


Figure 5.22: Temperature contours at $t = 30$

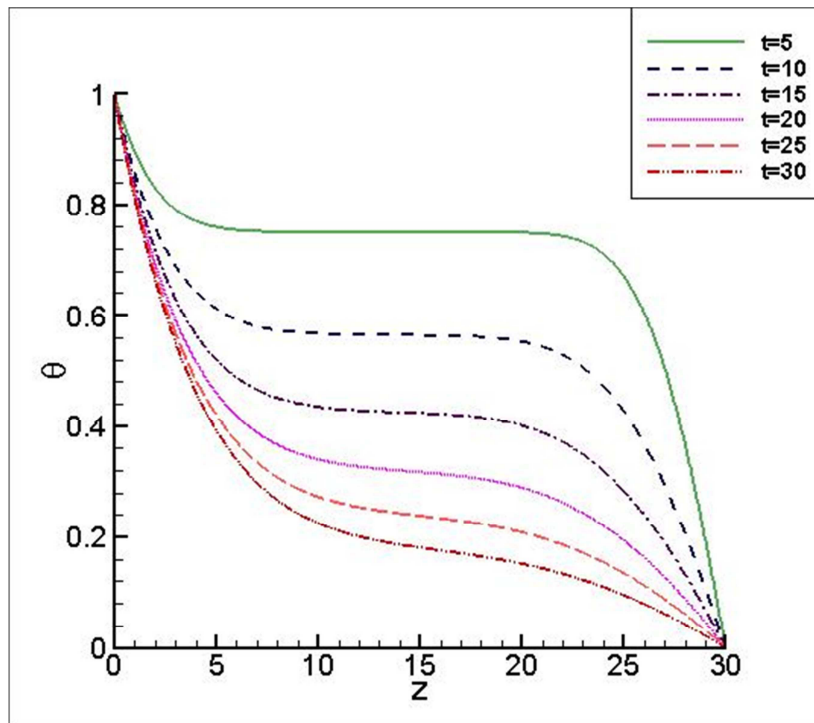


Figure 5.23: Surface temperature at different times

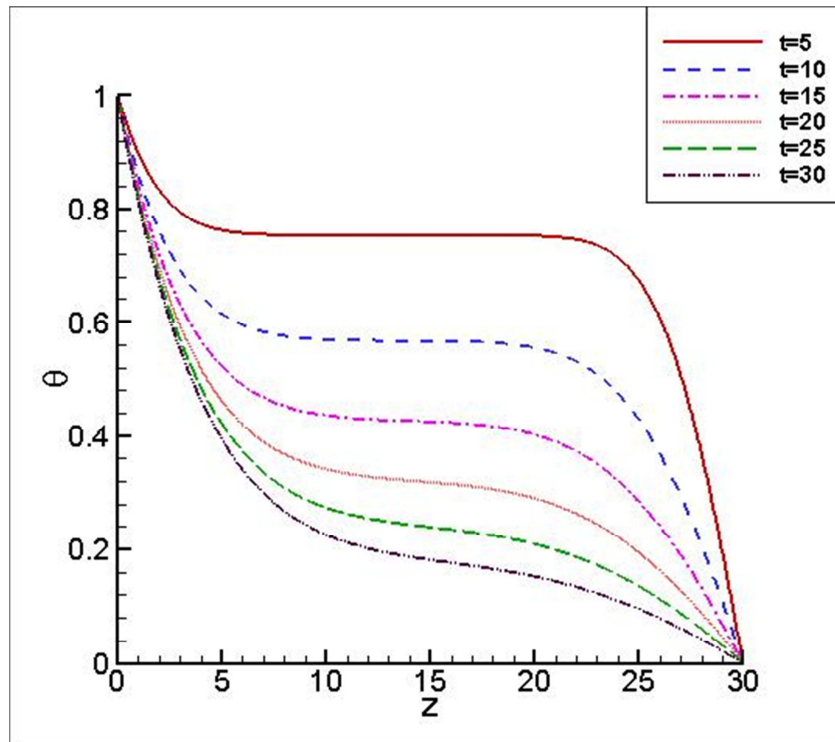


Figure 5.24: Center temperature at different times

The temperature contours are shown in Figures 5.25 and 5.26 for $Pe = 9.6661$, $Bi = 0.0119$. Surface and Center temperatures are shown in Figures 5.27 and 5.28 for $Pe = 9.6661$, $Bi = 0.0119$. For $Pe = 9.6661$ and $Bi = 0.0119$ the corresponding possible combinations of physical parameters are given by:

- Drawing velocity $U = 1.0$ cm/s and Diameter of fiber $D = 0.5$ mm.
- Drawing velocity $U = 0.5$ cm/s and diameter of fiber $D = 1.0$ mm

From Figures 5.25, 5.26, 5.27 and 5.28, one can notice that, the temperature values decreases with the increase of time means optical fiber cools as the time progress. The fiber temperature values are not changing much after $t = 30$. So steady state temperature of fiber is at $t = 30$.

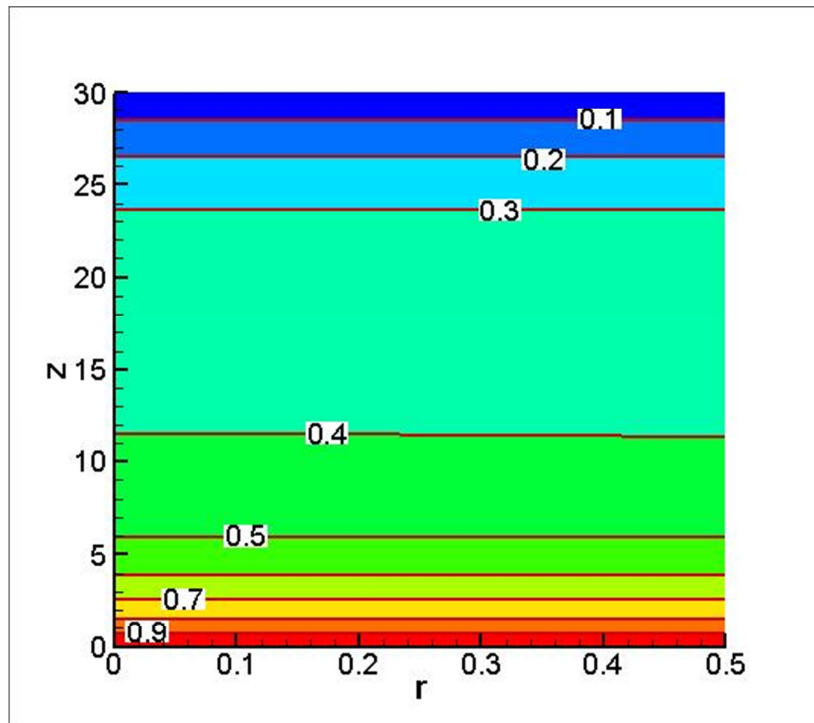


Figure 5.25: Temperature contours at $t = 20$

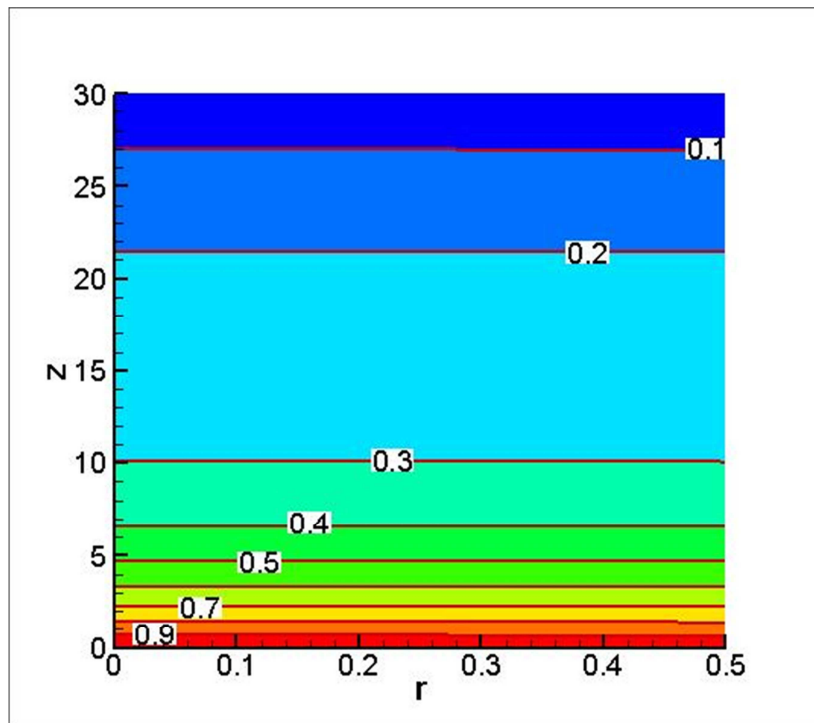


Figure 5.26: Temperature contours at $t = 30$

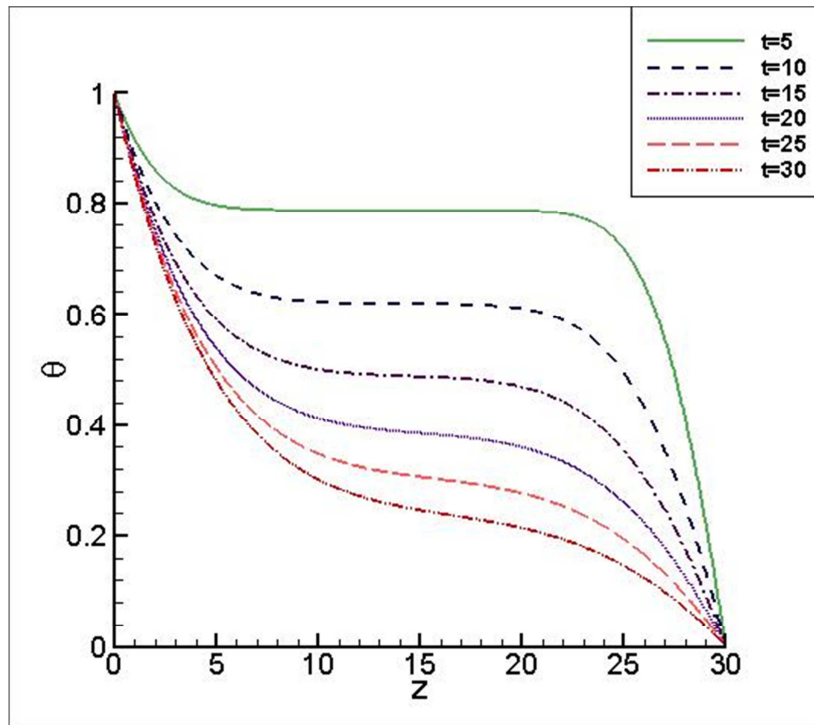


Figure 5.27: Surface temperature at different times

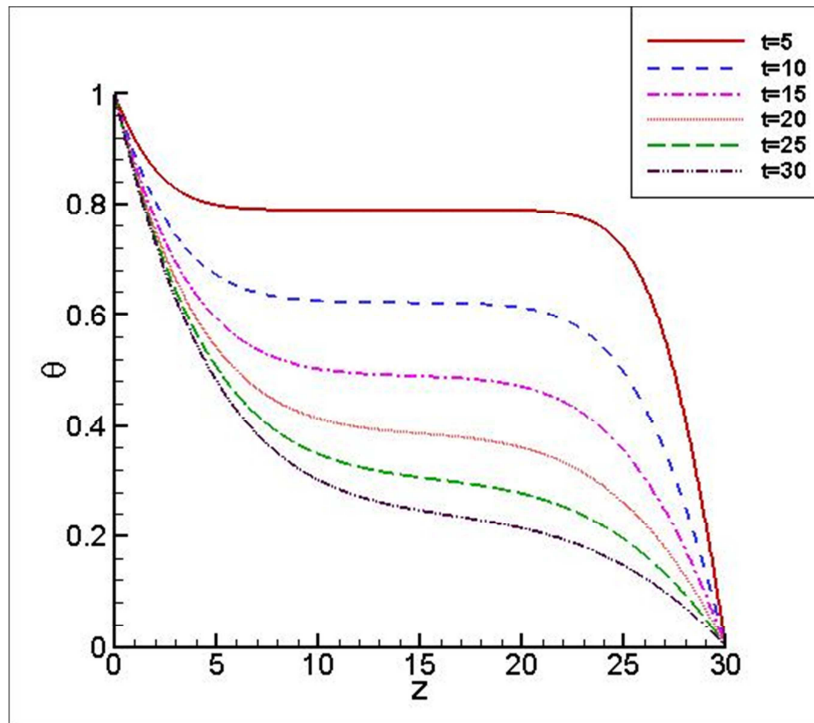


Figure 5.28: Center temperature at different time

5.2.3 Effect of drawing speed and size of optical fiber

From Table 5.3, the following three results will show the effect of drawing speed and diameter of the optical fiber:

- $Pe = 9.6661318$ and $Bi = 0.0119702$
- $Pe = 19.332264$ and $Bi = 0.0130932$
- $Pe = 28.998395$ and $Bi = 0.0142957$

The above three solutions corresponds to the physical parameters are:

- The constant drawing velocity $U_f = 1.0$ cm/s with varying diameters are $D = 0.5$ mm, 1.0 mm and 1.5 mm.
- The constant diameter $D = 1.0$ mm with varying drawing speeds are $U_f = 0.5$ cm/s, 1.0 cm/s and 1.5 cm/s.

The steady surface and center temperatures are shown in Figures 5.29 and 5.30 for the above three cases. From Figures 5.29 and 5.30, the surface and center temperature decreases with the increases of Pe means that faster cooling rate of the optical fiber with increasing Pe . The increasing of Pe and Bi corresponds to two physical situations as given above. As the diameter of the fiber increases keeping constant drawing velocity for the same fiber material corresponding Pe and Bi numbers increases. The surface temperature decreases with increase of Pe due to increase of surface area. So the cooling rate of the fiber is faster with the increase of diameter at a constant drawing speed of the fiber.

As the drawing velocity of the fiber increases keeping constant diameter for the same fiber material corresponding Pe and Bi numbers increases. The surface temperature decreases with increase of Pe due to increase of convective heat transfer coefficient. So the cooling rate of the fiber is faster with the increase of drawing velocity at a constant diameter of the fiber.

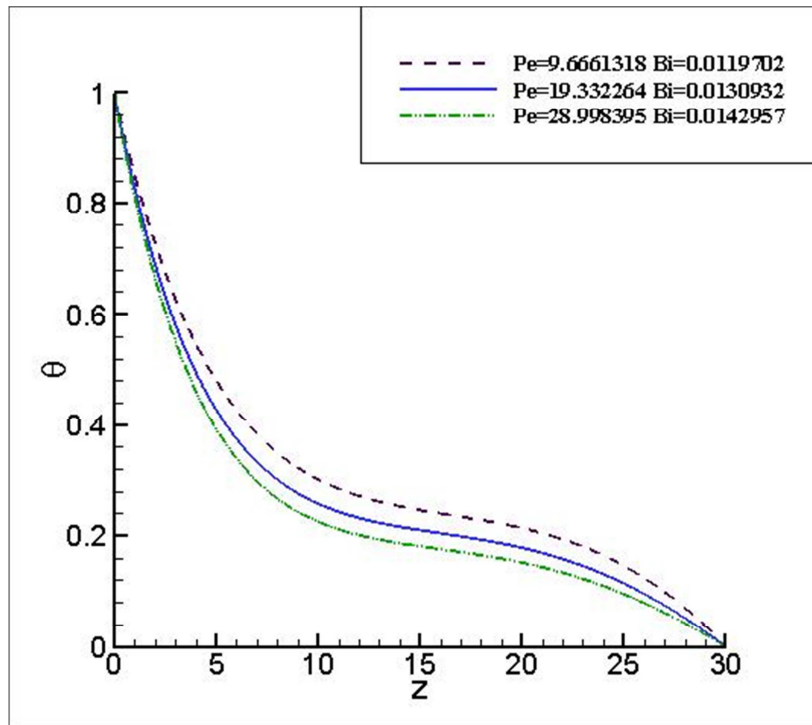


Figure 5.29: Comparison of surface temperatures at $t = 30$

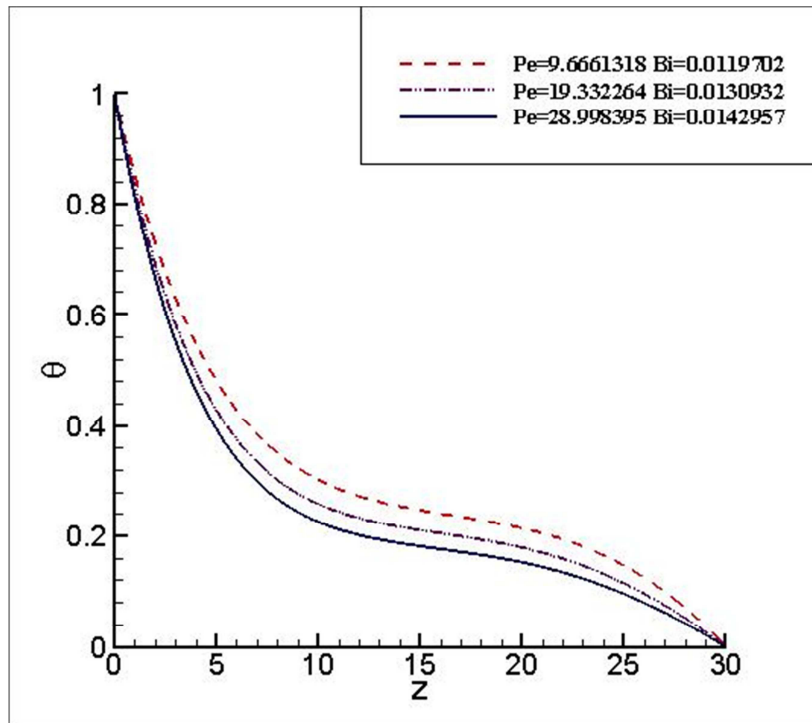


Figure 5.30: Comparison of center temperatures at $t = 30$

5.2.4 Effect of Bi number

Consider following two cases:

- $Pe = 19.3322$ with $Bi = 0.0227$ and $h = 25.3817$ (w/m^2k)
- $Pe = 19.3322$ with $Bi = 0.0455$ and $h = 50.7634$ (w/m^2k)

For both cases speed is constant 1.0 cm/s and diameter is also constant 1.0 mm. Because of increasing h value as double; Bi number is double. For both cases Pe number is same and Bi number of second case is exactly double compared to first case.

From Figures 5.31 and 5.32, the surface and center temperature decreases with the increases of Bi means that faster cooling rate of the optical fiber with increasing Bi . As Bi number increases, Convective heat transfer coefficient increases, surface temperature decreases and fiber cools quickly.

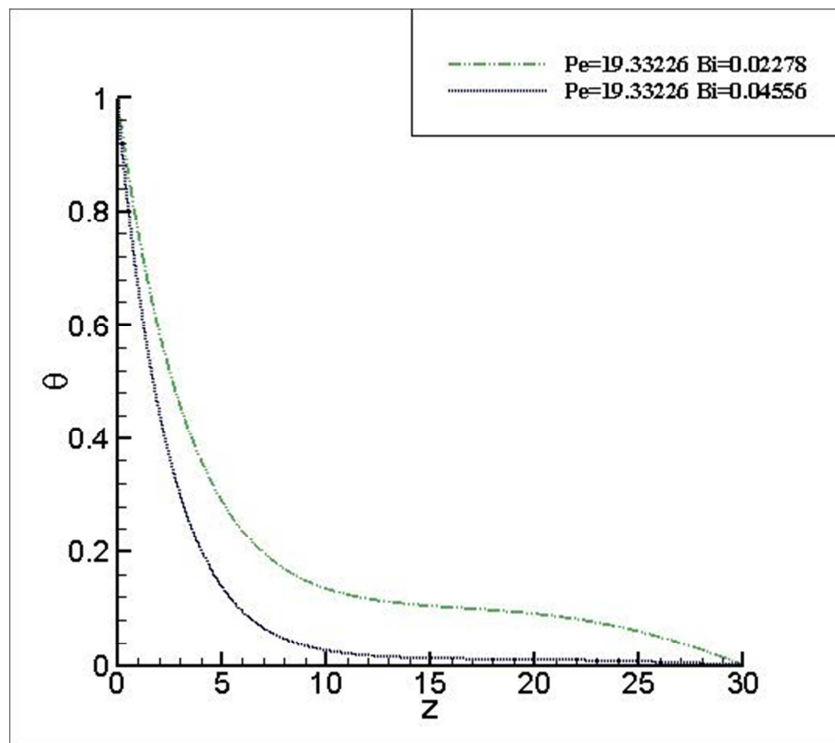


Figure 5.31: Comparison of surface temperatures at $t = 25$

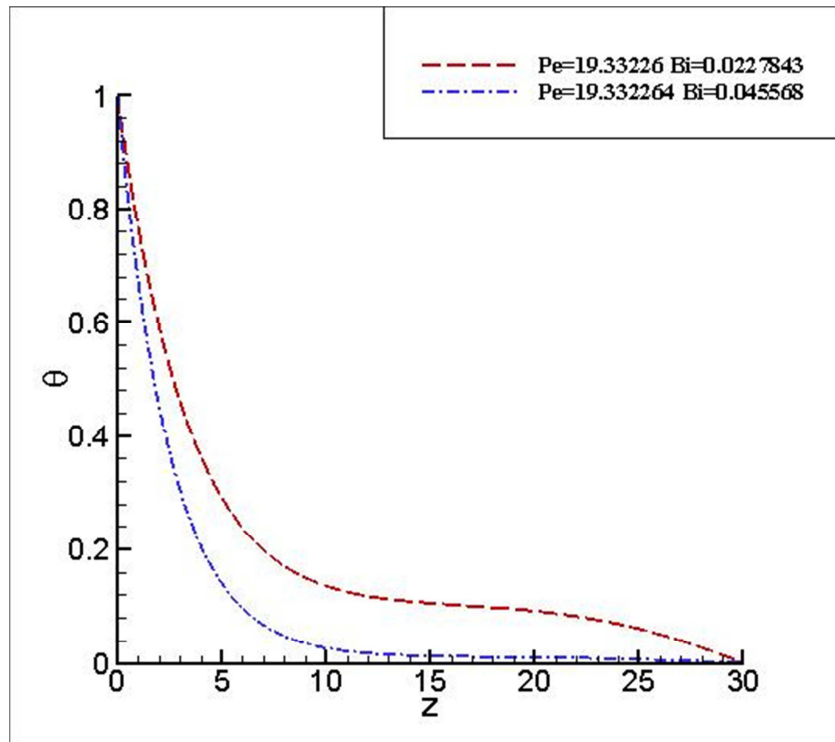


Figure 5.32: Comparison of center temperatures $t = 25$

5.2.5 Effect of Pe number

Consider following two cases:

- $Pe = 19.3322$ with $Bi = 0.0227$ and $h = 25.3817(\text{w/m}^2\text{k})$
- $Pe = 38.6639$ with $Bi = 0.0227$ and $h = 25.3817(\text{w/m}^2\text{k})$

For both cases Bi number is same and Pe number of second case is exactly double compared as first case. $Pe = 19.3322$ with $Bi = 0.0227$ corresponds speed 1.0 cm/s and diameter of fiber 1.0 mm. $Pe = 38.6639$ with $Bi = 0.0227$ corresponds speed 2.0 cm/s and diameter of fiber 1.0 mm. Because of increasing speed as double; Pe number is double.

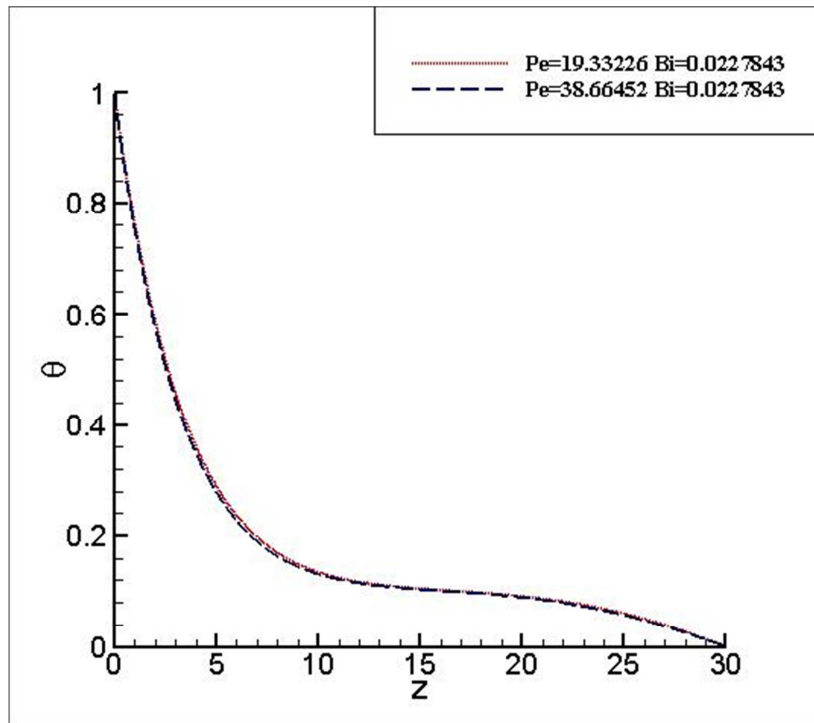


Figure 5.33: Comparison of surface temperatures at $t = 25$

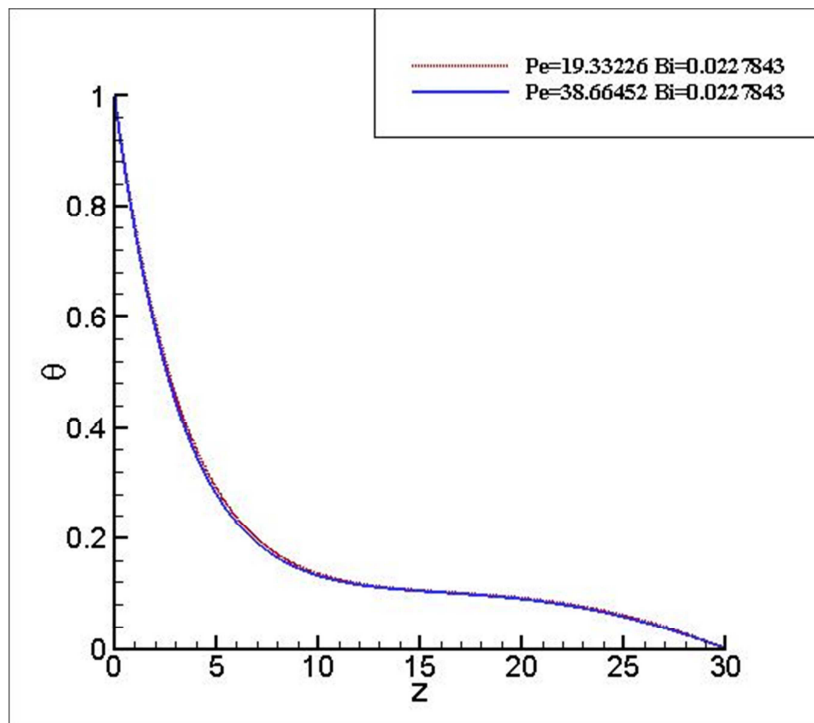


Figure 5.34: Comparison of center temperatures at $t = 25$

From Figures 5.33 and 5.34, the surface and center temperature decreases with the increases of Pe means that faster cooling rate of the optical fiber with increasing speed. Surface area increases, Surface temperature decreases and fiber cools quickly.

5.2.6 Effect of high drawing speed of fiber

As the velocity of the fiber increases from 1.0 cm /s to 1.0 m/s with a fixed diameter of the fiber is 1.0 mm corresponding dimensionless numbers increases from $Pe = 19.3322$ to 1933.22 and Bi increases from $Bi = 0.0130$ to 0.8276 as shown in Table 5.3.

From Figures 5.35 and 5.36, the surface and center temperature decreases with the increases of drawing velocity. As the drawing velocity of the fiber increases keeping constant diameter for the same fiber material corresponding Pe and Bi numbers increases. The surface temperature decreases with increase of Pe due to increase of convective heat transfer coefficient. So the cooling rate of the fiber is faster with the increase of drawing velocity at a constant diameter of the fiber.

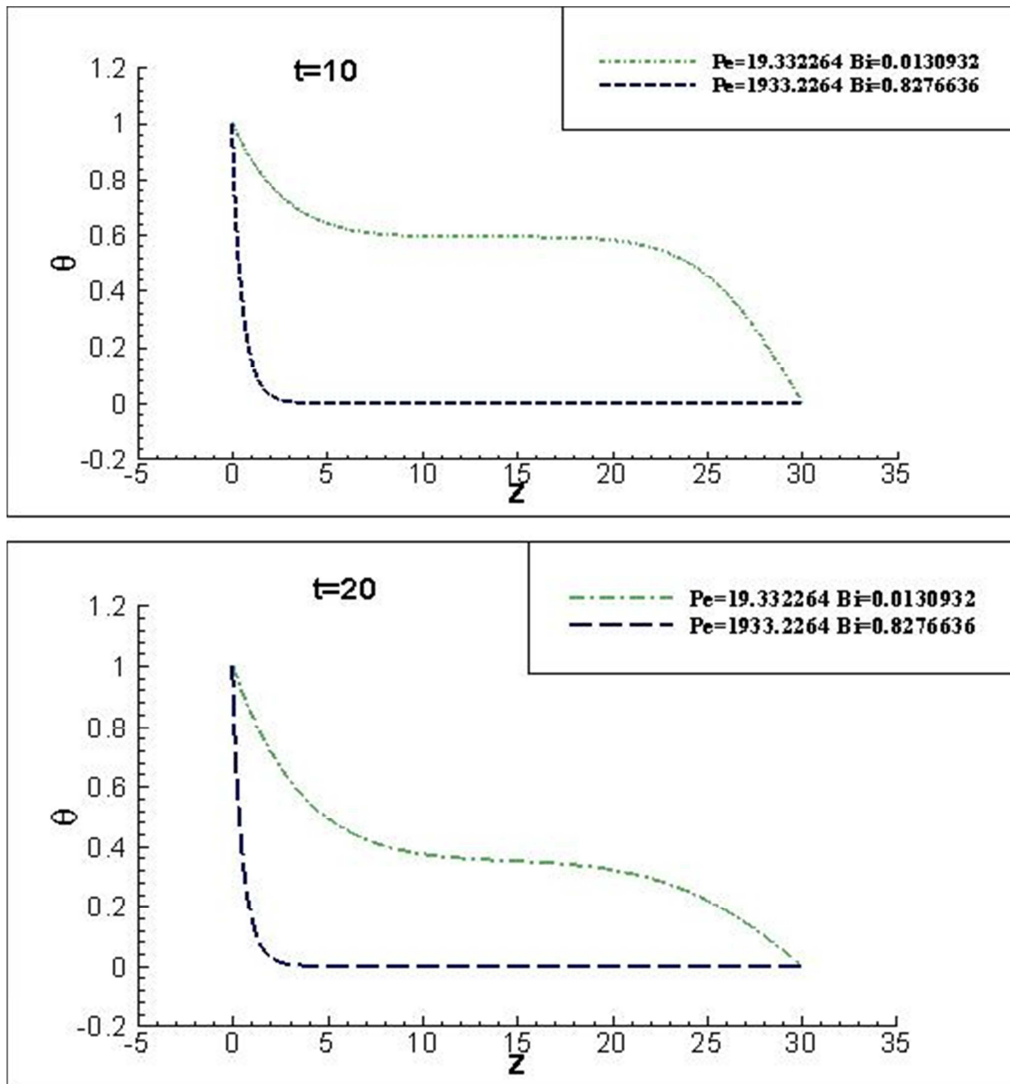


Figure 5.35: Comparison of surface temperatures at $t = 10$ and 20

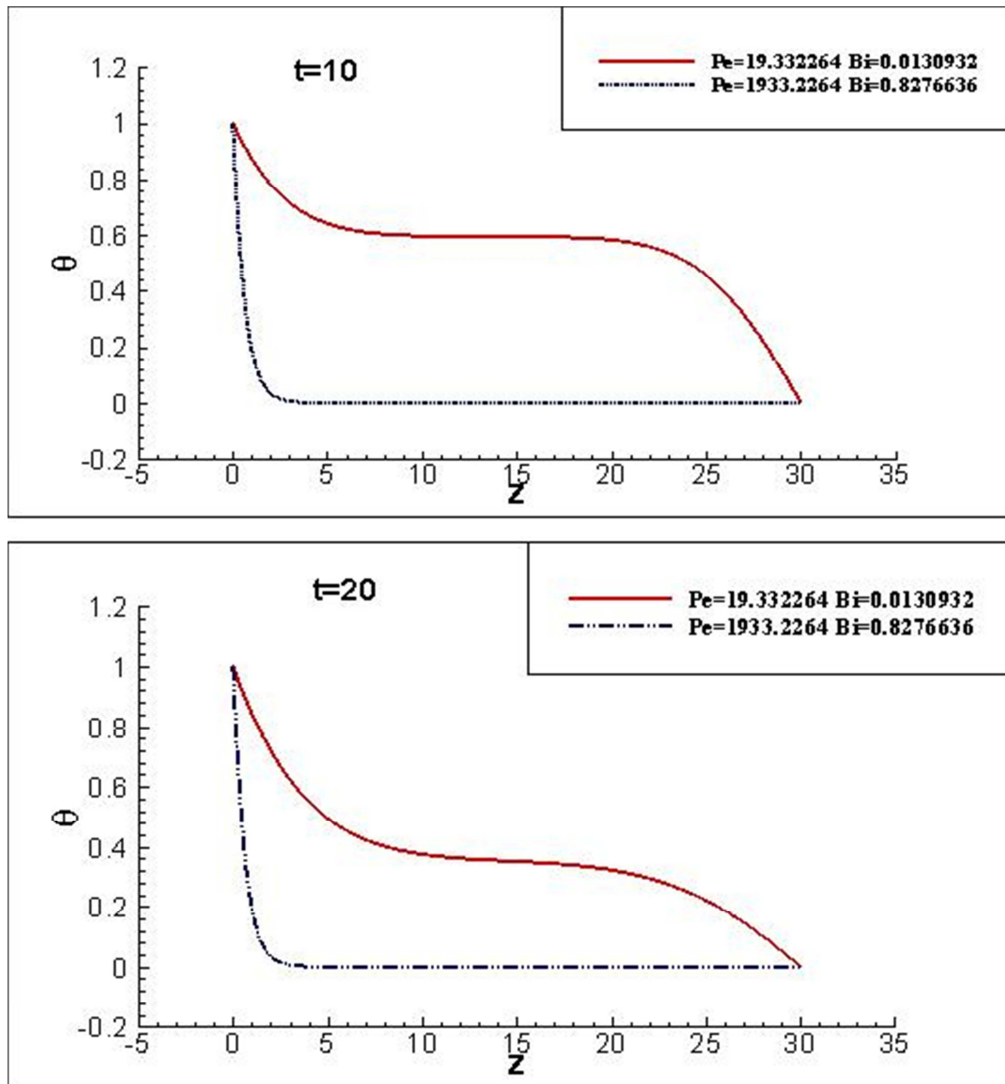


Figure 5.36: Comparison of center temperatures at $t = 10$ and 20

5.2.7 Effect of thick fiber

As the diameter of the fiber increases from 1.0 mm to 3.0 mm with a constant drawing speed of the fiber is 1.0 m/s corresponding dimensionless numbers increases from $Pe = 1933.2264$ to 5799.6791 and Bi increases from $Bi = 0.8276$ to 2.0797 as shown in Table 5.3. From Figures 5.37 and 5.38, the surface and center temperature decreases with the increases of Pe means that faster cooling rate of the optical fiber with increasing Pe . The increasing of Pe and Bi corresponds to two physical situations as given above. As the diameter of the fiber increases keeping constant drawing velocity for the same fiber material corresponding Pe and Bi numbers increases. The surface temperature decreases with increase of Pe due to

increase of surface area. So the cooling rate of the fiber is faster with the increase of diameter at a constant drawing speed of the fiber.

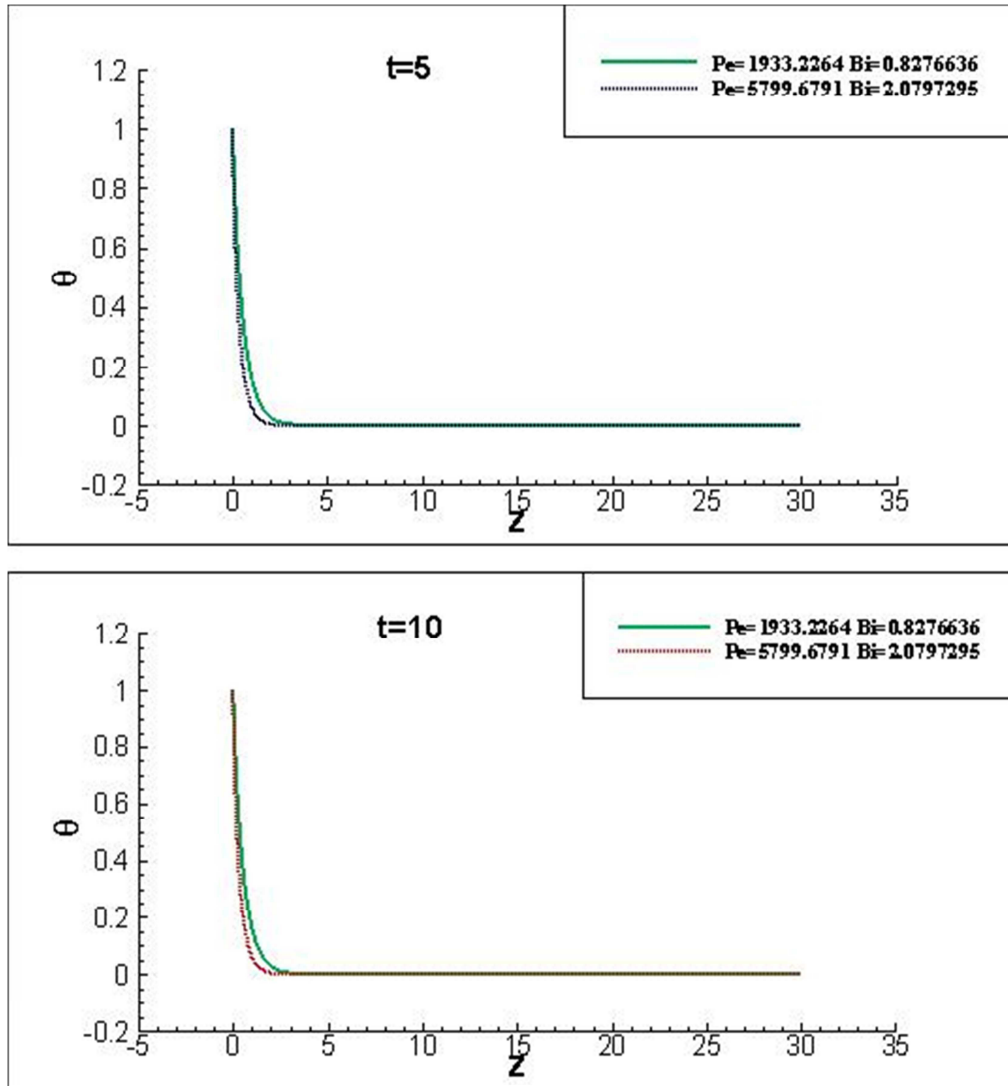


Figure 5.37: Comparison of surface temperatures at $t = 5$ and 10

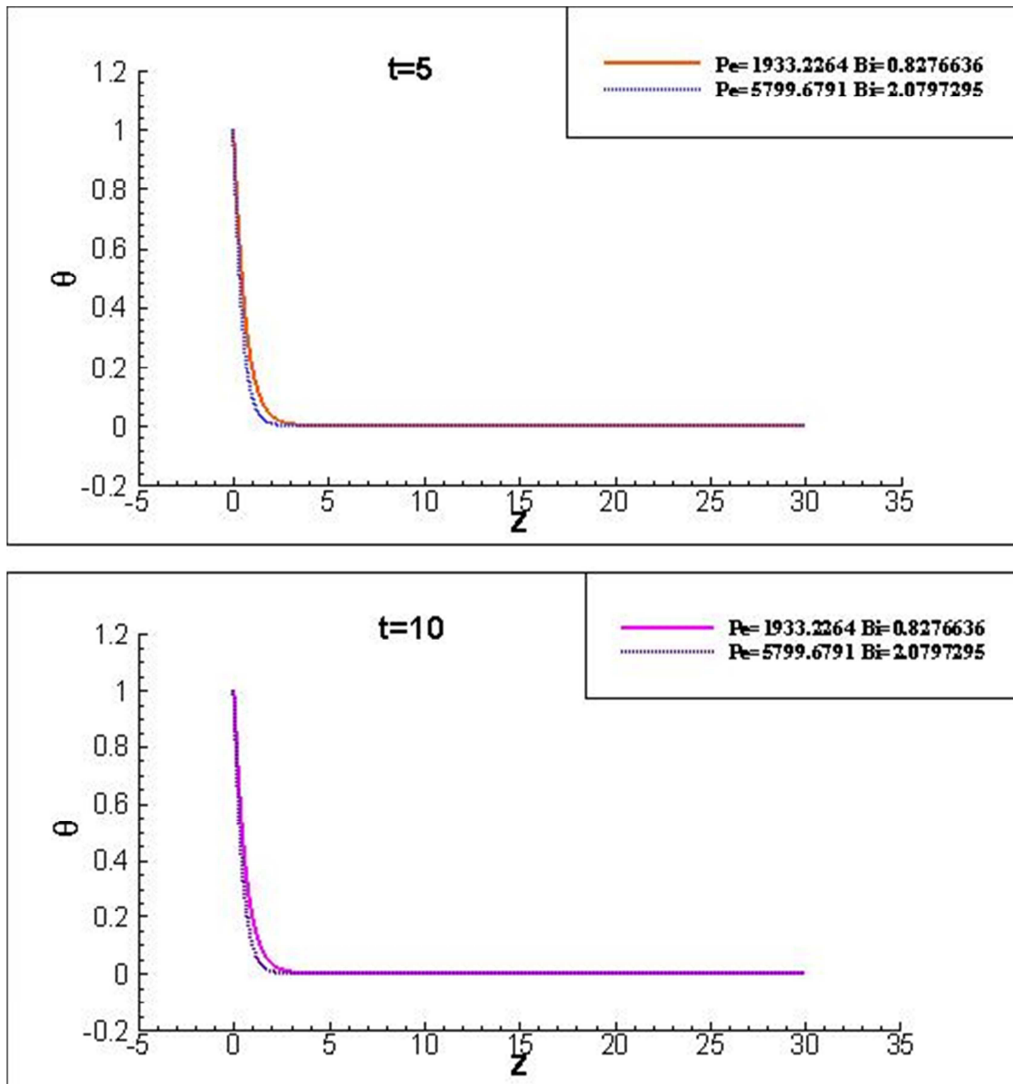


Figure 5.38: Comparison of center temperatures at $t = 5$ and 10

5.2.8 Effect of material

The diameter and drawing speed of the VYCOR optical fiber are 1.0 mm and 1.0 cm/s corresponding dimensionless numbers are $Pe = 11.8478$ and $Bi = 0.0105$ as given in Table 5.3. The average convective heat transfer coefficient is obtained from the boundary layer solution as discussed in previous section 4.1. The temperature contours are shown in Figure 5.39 with different times $t = 5, 10, 20,$ and 30 for the case of $Pe = 11.8478$ with $Bi = 0.0105$. The surface and center temperatures with different times for the case of $Pe = 11.8478$ and $Bi = 0.0105$ as shown in Figures 5.40 and 5.41.

From Figures 5.39, 5.40, and 5.41, one can notice that , the temperature values decreases with the increase of time means optical fiber cools as the time progress. The fiber temperature values are not changing much after $t = 30$. So steady state temperature of fiber is at $t = 30$.

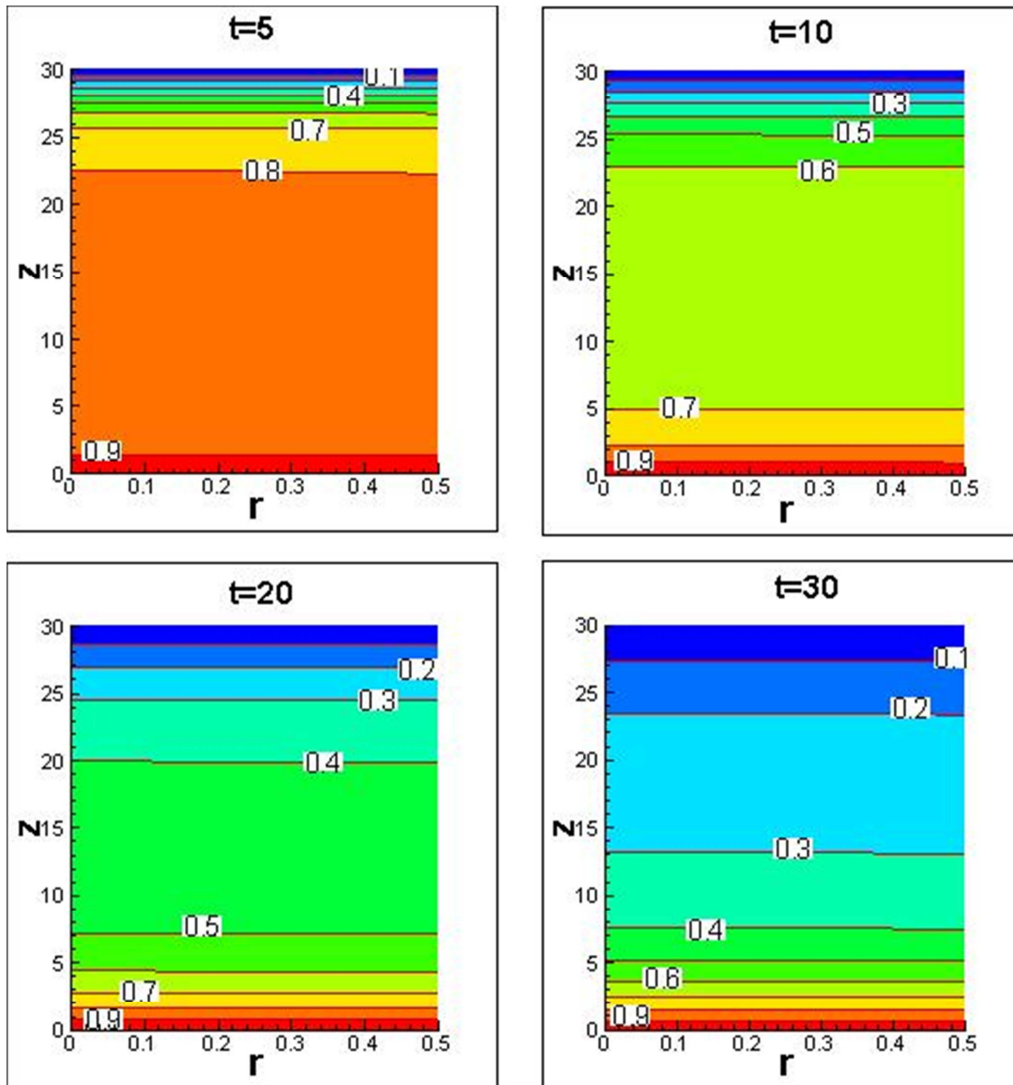


Figure 5.39: Temperature contours at $t = 5, 10, 20$ and 30

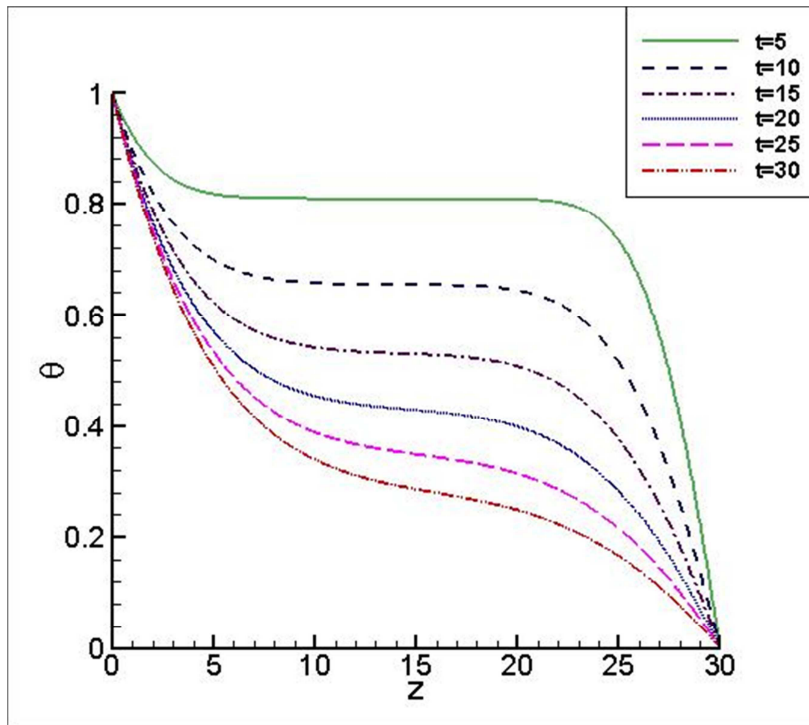


Figure 5.40: Surface temperatures at different time

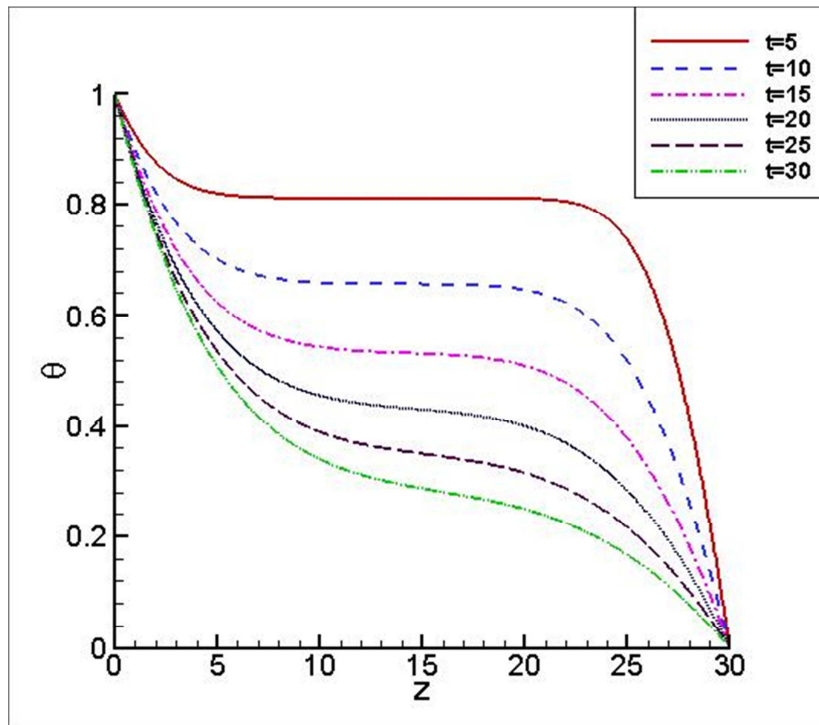


Figure 5.41: Center temperature at different time

The temperature contours are shown in Figures 5.42 and 5.43 for $Pe = 17.7717$, $Bi = 0.0115$. Surface and Center temperatures are shown in Figures 5.44 and 5.45 for $Pe = 17.7717$, $Bi = 0.0115$. For $Pe = 17.7717$ and $Bi = 0.0115$ the corresponding possible combinations of physical parameters are given by:

- Drawing velocity $U = 1.0$ cm/s and Diameter of fiber $D = 1.5$ mm
- Drawing velocity $U = 1.5$ cm/s and Diameter of fiber $D = 1.0$ mm

From Figures 5.42, 5.43, 5.44 and 5.45, one can notice that , the temperature values decreases with the increase of time means optical fiber cools as the time progress. The fiber temperature values are not changing much after $t = 30$. So steady state temperature of fiber is at $t = 30$.

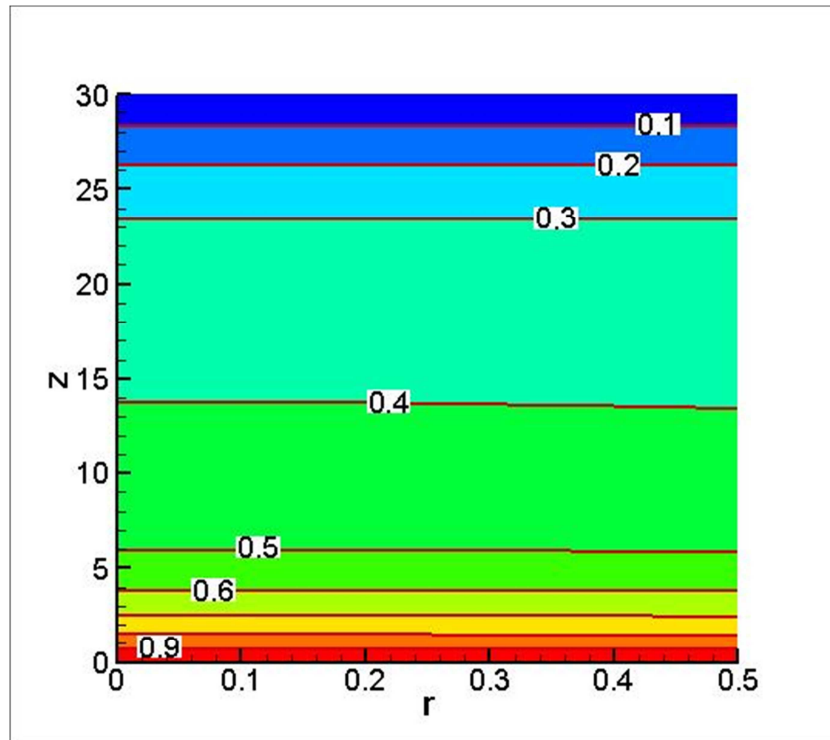


Figure 5.42: Temperature contours at $t = 20$

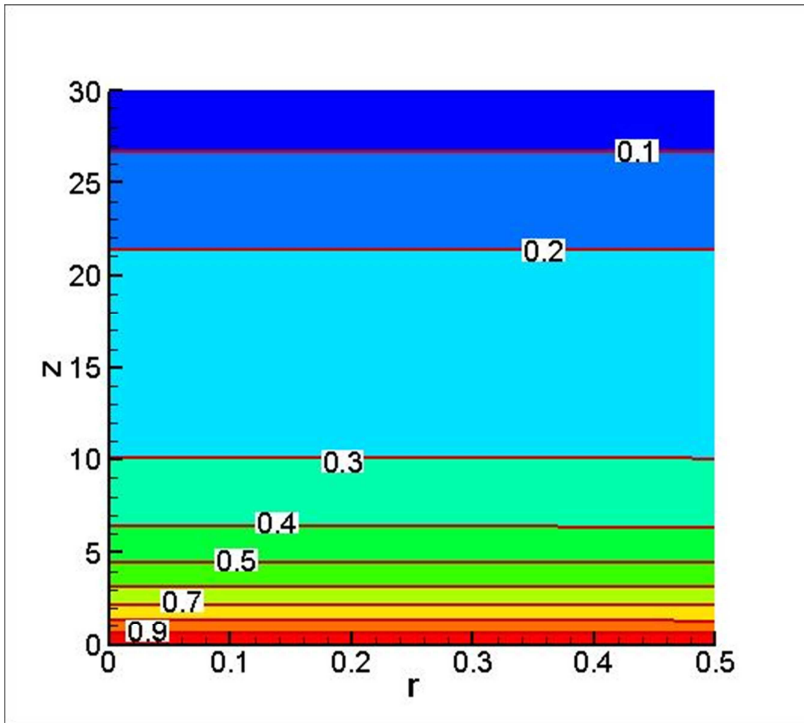


Figure 5.43: Temperature contours at $t = 30$

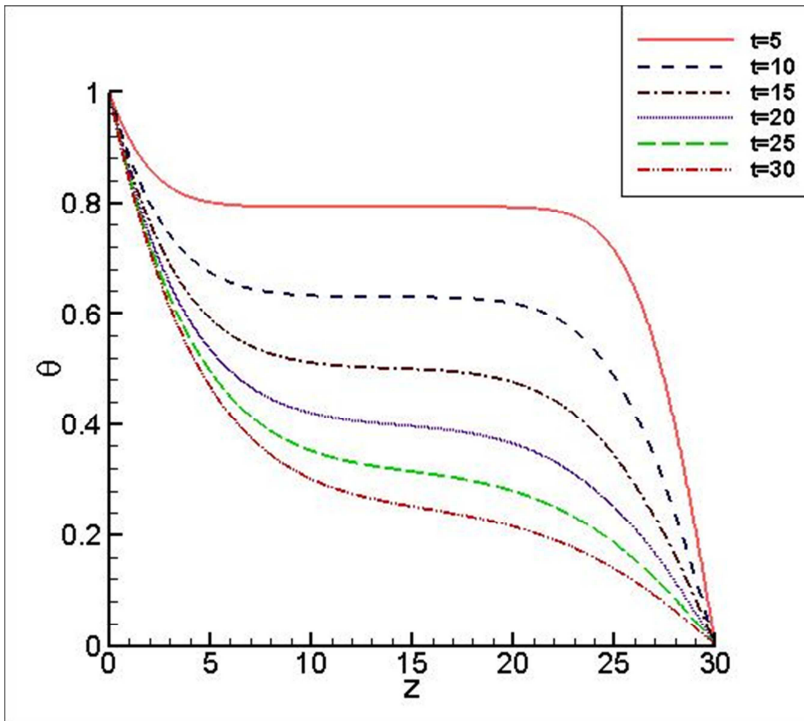


Figure 5.44: Surface temperatures at different time

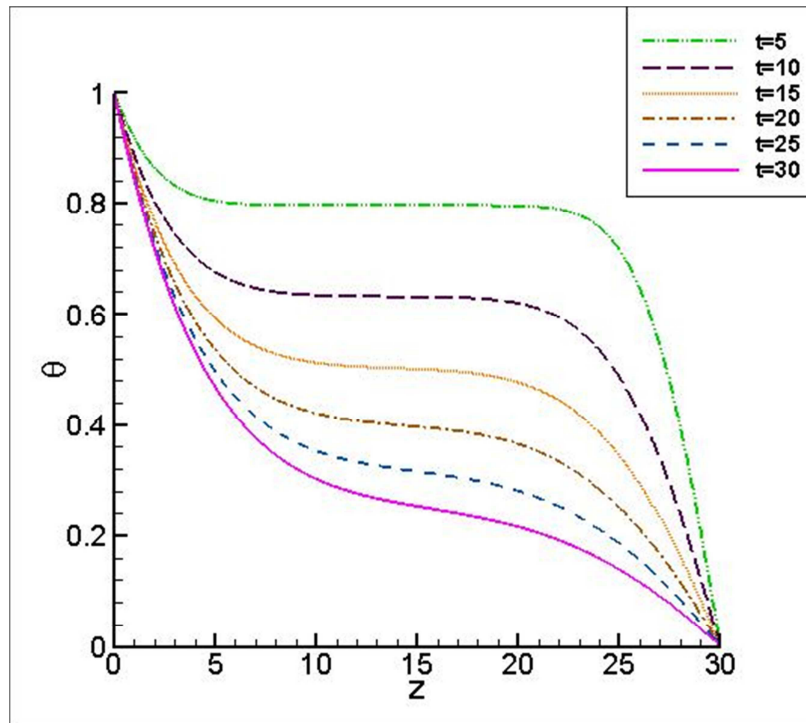


Figure 5.45: Center temperatures at different time

From the Table 5.3, the following three results will show the effect of drawing speed and diameter of the optical fiber:

- $Pe = 5.923913$ and $Bi = 0.009662$
- $Pe = 11.84782$ and $Bi = 0.010569$
- $Pe = 17.77173$ and $Bi = 0.011540$

The above three solutions corresponds to the physical parameters are:

- The constant drawing velocity $U_f = 1.0$ cm/s with varying diameters are $D = 0.5$ mm, 1.0 mm and 1.5 mm.
- The constant diameter $D = 1.0$ mm with varying drawing speeds are $U_f = 0.5$ cm/s, 1.0 cm/s and 1.5 cm/s.

The steady surface and center temperatures are shown in Figures 5.46 and 5.47 for the above three cases.

From Figures 5.46 and 5.47, the surface and center temperature decreases with the increases of Pe means that faster cooling rate of the optical fiber with increasing Pe . The increasing of Pe and Bi corresponds to two physical situations as given above. As the diameter of the fiber increases keeping constant drawing velocity for the same fiber material corresponding

Pe and Bi numbers increases. The surface temperature decreases with increase of Pe due to increase of surface area. So the cooling rate of the fiber is faster with the increase of diameter at a constant drawing speed of the fiber.

As the drawing velocity of the fiber increases keeping constant diameter for the same fiber material corresponding Pe and Bi numbers increases. The surface temperature decreases with increase of Pe due to increase of convective heat transfer coefficient. So the cooling rate of the fiber is faster with the increase of drawing velocity at a constant diameter of the fiber.

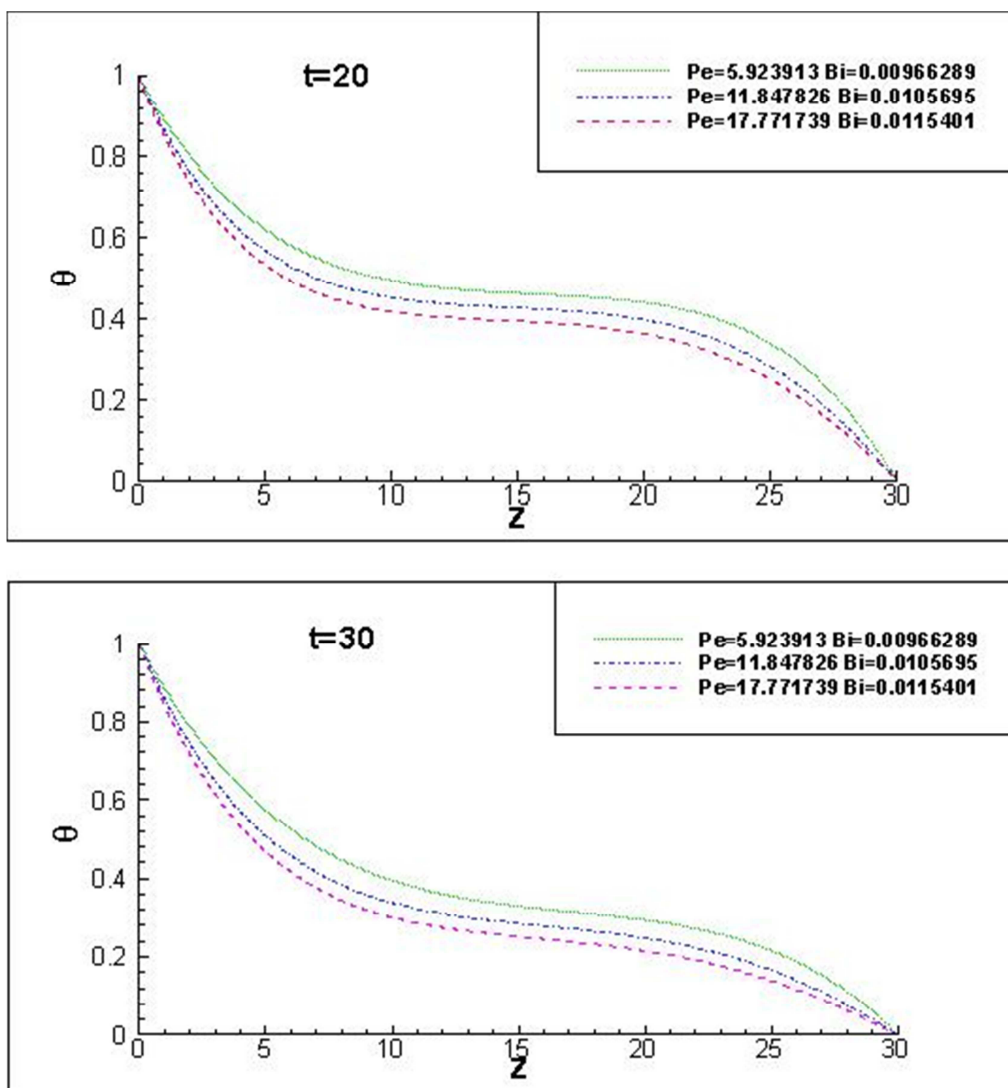


Figure 5.46: Comparison of surface temperatures at $t = 20$ and 30

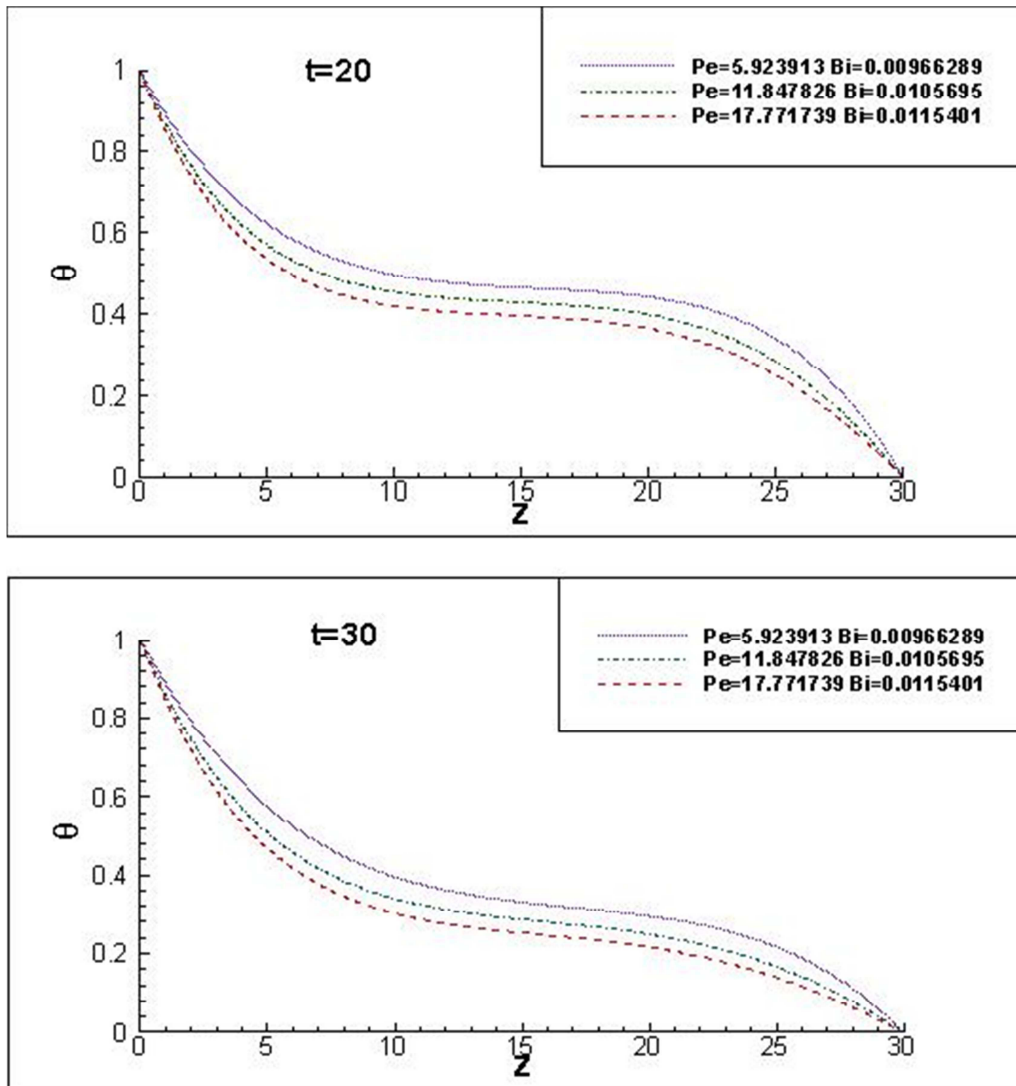


Figure 5.46: Comparison of center temperatures at $t = 20$ and 30

5.2.9 Effect of thermal conductivity

The two different material of fiber are BK7 and VYCOR with a same drawing speed and diameter of the fiber are 0.5 cm/s and 1.0 mm corresponding dimensionless numbers decreases from $Pe = 9.6661$ to 5.9239 and Bi from $Bi = 0.0119$ to 0.0096 as shown in Table 5.3. As the material of the fiber changes from BK7 to VYCOR; correspondingly thermal conductivity increases from $\kappa = \text{value to value}$. The surface and center temperature profiles of the two fibers are given in Figure 5.47. From Figure, the surface temperature and center temperature increases with decrease of Pe and Bi . As previously explained that fiber cooling rate is faster with increase of Pe and Bi . So the cooling rate of the fiber is slower as

the thermal conductivity of fiber increases with constant drawing speed and size of the fibers.

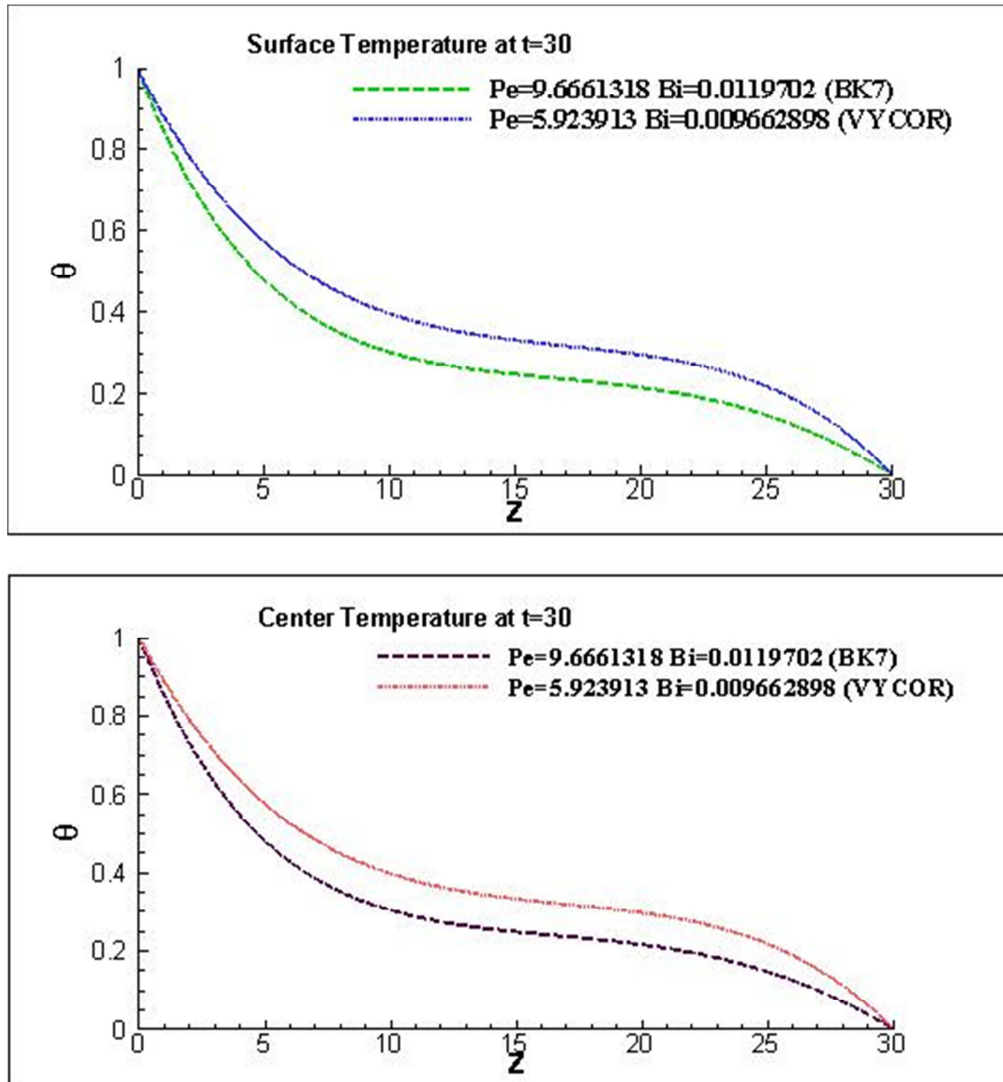


Figure 5.47: Surface and center temperature when $U = 0.5$ cm/s and $D = 1.0$ mm

The two different material of fiber are BK7 and VYCOR with a same drawing speed and diameter of the fiber are 1.0 cm/s and 1.0 mm corresponding dimensionless numbers decreases from $Pe = 19.3322$ to 11.8478 and Bi from $Bi = 0.0130$ to 0.0105 as shown in Table 5.3. As the material of the fiber changes from BK7 to VYCOR; correspondingly thermal conductivity increases from $\kappa =$ value to value. The surface and center temperature profiles of the two fibers are given in Figure 5.48. From Figure, the surface temperature and center temperature increases with decrease of Pe and Bi . As previously explained that fiber cooling rate is faster with increase of Pe and Bi . So the cooling rate of the fiber is slower as

the thermal conductivity of fiber increases with constant drawing speed and size of the fibers.

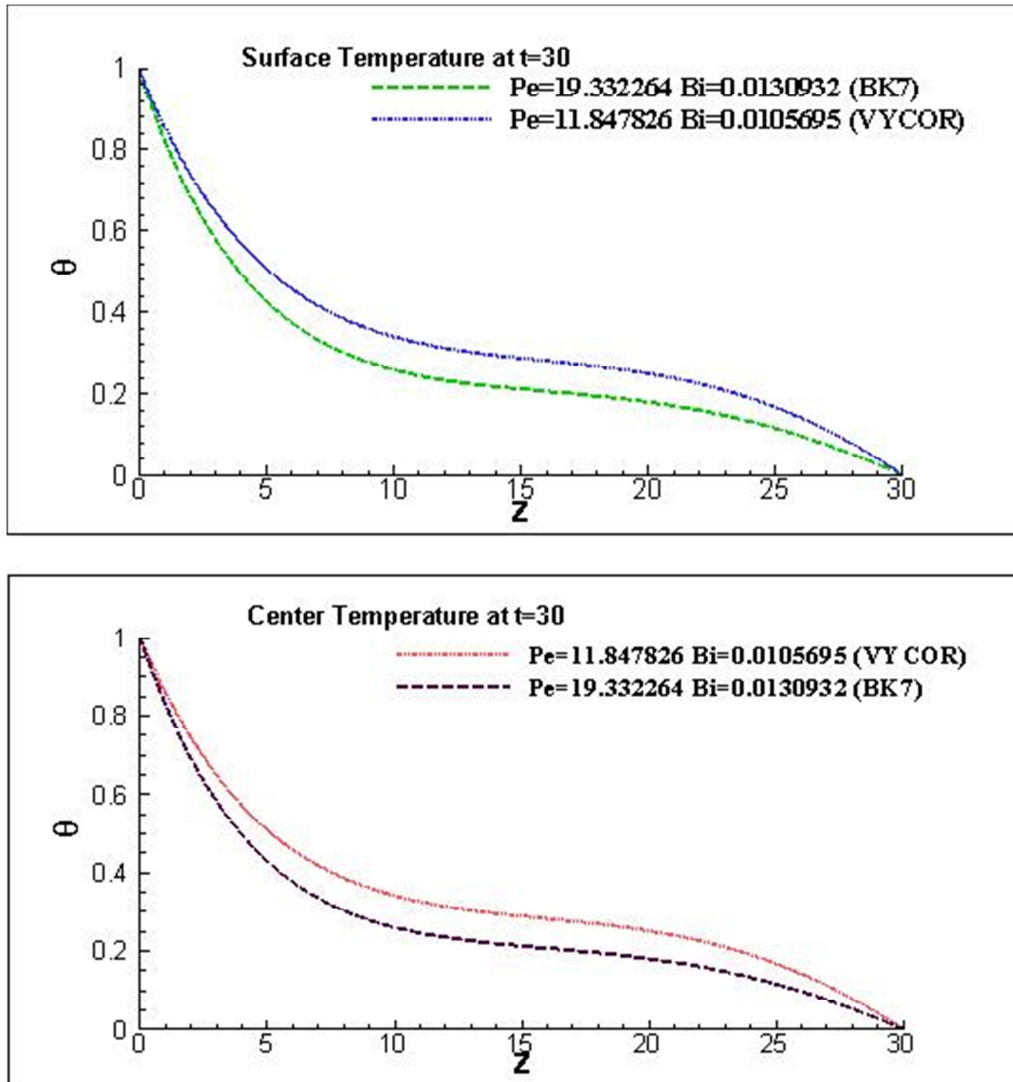


Figure 5.48: Surface and center temperature when $U = 1.0$ cm/s and $D = 1.0$ mm

The two different material of fiber are BK7 and VYCOR with a same drawing speed and diameter of the fiber are 1.5 cm/s and 1.0 mm corresponding dimensionless numbers decreases from $Pe = 28.9983$ to 17.7717 and Bi from $Bi = 0.0142$ to 0.0115 as shown in Table 5.3. As the material of the fiber changes from BK7 to VYCOR; correspondingly thermal conductivity increases from $\kappa =$ value to value. The surface and center temperature profiles of the two fibers are given in Figure 5.49. From Figure, the surface temperature and center temperature increases with decrease of Pe and Bi. As previously explained that fiber cooling rate is faster with increase of Pe and Bi. So the cooling rate of the fiber is slower as

the thermal conductivity of fiber increases with constant drawing speed and size of the fibers.

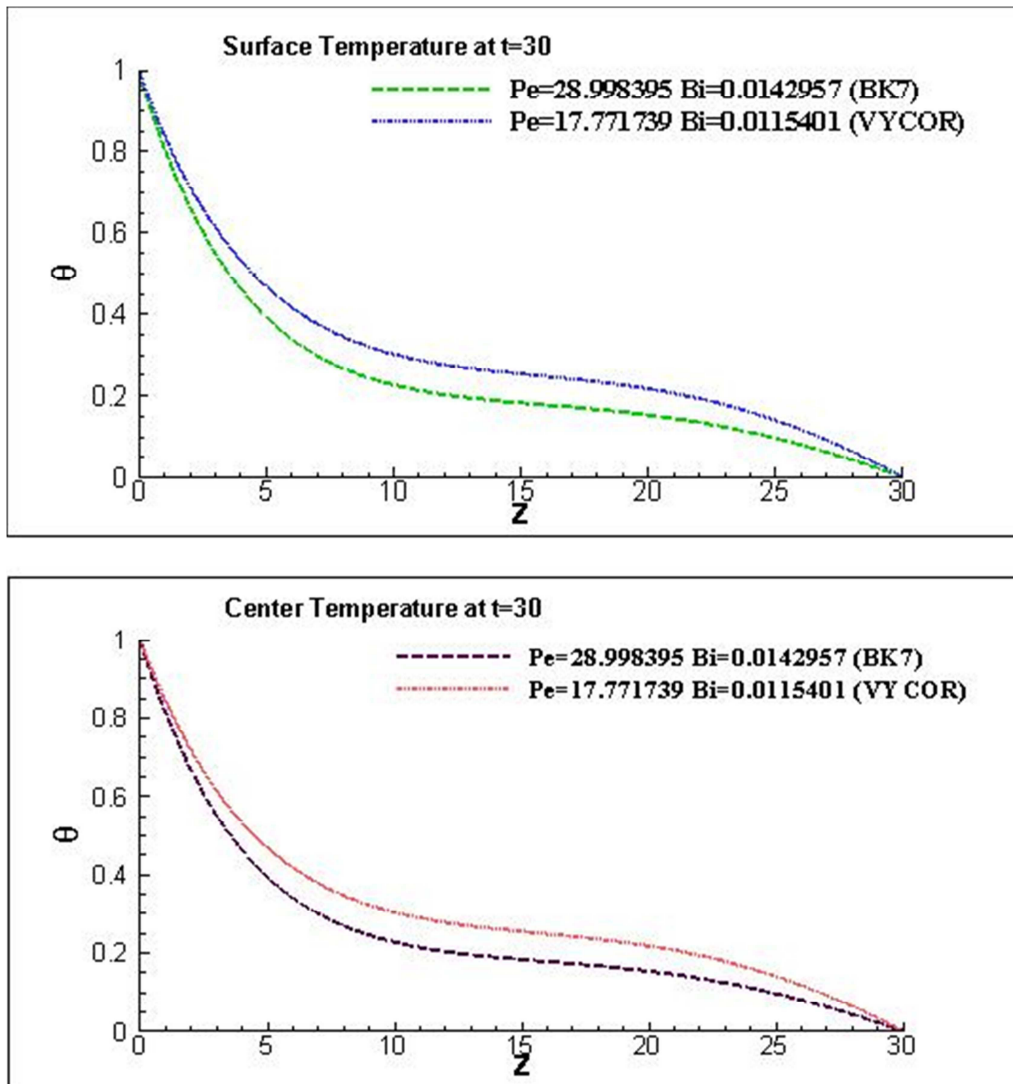


Figure 5.49: Surface and center temperature when $U = 1.5 \text{ cm/s}$ and $D = 1.0 \text{ mm}$

Low thermal conductivity material (BK7) cools quickly as compared to high thermal conductivity material (VYCOR) having same drawing velocity as well as diameter for both materials.

Reported results show cooling of optical fibers is faster by increasing drawing velocity of the fiber with a fixed diameter or by increasing diameter of the fiber with a constant drawing velocity. Cooling of the optical fibers is slow with the increase of thermal conductivity of the fiber for a fixed size and drawing speed of the fiber.

Chapter 6

Conclusions

The thermal behavior of optical fibers during the cooling stage of the drawing process has been investigated and reported here. Results are given for different diameter and drawing speed of the fiber. The diameter of fiber varies from 0.5 to 3.0 mm and drawing speed varies from 1.0 cm/s to 1.0 m/s. Convection as well as conduction models of optical fibers during the cooling stage of the drawing process have been studied and reported the surface and center temperature of the fibers. Results are reported for two common materials of fiber are BK7 and VYCOR. High accuracy implicit finite difference method is used to obtain the value of convective heat transfer coefficient at the surface of the fiber. Present numerical approach is good accuracy compared to integral approach reported in the literature to obtain the convective heat transfer coefficient at the surface of the fiber.

From the results we have given the following conclusions:

- If fiber material is same, as the diameter of the fiber increases keeping drawing velocity as constant Pe number as well as Bi number increases. Therefore surface area increases, surface temperature decreases and fiber cools quickly.
- If fiber material is same, as drawing velocity increases keeping diameter as constant Pe number as well as Bi number increases. Convective heat transfer coefficient increases, surface temperature decreases and fiber cools quickly.
- For same fiber material if either drawing velocity is very high or diameter is very thick then convective heat transfer coefficient increases and surface temperature decreases. Therefore fiber cool more quickly compared to other cases.
- For same fiber materials, for the combination of velocities and diameters having either high Pe number or Bi number gives better cooling of fiber.

- Low thermal conductivity material (BK7) cools quickly as compared to high thermal conductivity material (VYCOR) having same drawing velocity as well as diameter for both materials.

6.1 Future Work

Temperature distribution for a single rod thick fiber has been examined. Data is collected for diameter ranging from 0.5 to 3.0 mm and drawing speed from 1.0 cm/s to 1.0 m/s. Results show drawing velocity and diameter of the fiber play an important role in cooling of optical fiber. We have seen that cooling of optical fiber is very fast if drawing velocity is very high. We suggest that the present work can be extended for very high drawing speed of the fiber may be up to 30 m/s. We also suggest that one can study the thermal behavior of hollow glass optical fibers.

References

- [1] G.W. McLellan and E. B. Shand, Glass Engineering Handbook, McGraw-Hill, New York, 1984.
- [2] O. L. Anderson, Conjugate heat transfer of continuously moving surfaces, J. Appl. Phys. 29, 9-12, 1958.
- [3] Glicksman L. R., The cooling of glass fibers. Glass Technology 9(5), 131-138, and 1968.
- [4] Bourne and D. G. Elliston, Heat transfer through the axially symmetric boundary layer on a moving circular fiber, Int. J. Heat Mass Transfer 13, 583-593, 1970.
- [5] Bourne and H. Dixon, The cooling of fibers in the formation process, J. Heat Mass Transfer 24, 1323-1331, 1971.
- [6] U. C. Paek and R. B. Runk, Physical Behavior of the Neck-Down Region during Furnace Drawing of Silica Fibers, J. of Applied Physics vol. 49, pp. 4417-4422, 1978.
- [7] M. Homsy and K. Walker, Heat Transfer in Laser Drawing of Optical Fibers, Glass Technol. vol. 20, no. 1, pp. 20] 26, 1979.
- [8] R. Sayles and B. Casewell, A Finite Element Analysis of the Upper Jet Region of a Fiber Drawing Flow Field of a Temperature Sensitive Material, Int. J. of Heat & Mass Transfer, vol. 27, pp. 57-67, 1984.
- [9] M. R. Myers, A Model for Unsteady Analysis of Preform Drawing, AIChE Journal. vol. 35, no. 4, pp. 592-602, 1989.
- [10] Haris Papamichael and Ioannis N. Miaoulisa, Thermal behavior of optical fibers during the cooling stage of drawing process, 1990.
- [11] S. Roy Choudhury and Y. Jaluria, Analytical solution for the transient temperature distribution in a moving rod or plate of finite length with surface heat transfer, 1993.
- [12] Z. Yin and Y. Jaluria, Thermal Transport and Material Flow in High Speed Optical Fiber Drawing, J. Heat Transfer. vol. 120, pp. 916- 930, 1998.

- [13] Hanafusa. Y. Hibino. and F. Yamamoto, Formation Mechanism of Drawing-Induced E Centers in Silica Optical Fibers, *J. Appl. Phys.* vol. 58, no. 3, pp. 1356, 1361, 1985.
- [14] Prof. Dr. Fedor Mitschke, *Fiber Optics Physics and Technology*, Springer Publication. University at Rostock, 18055 Rostock Germany.
- [15] Incropera DeWitt, *Fundamental of Heat and Mass Transfer*, 6th edition.
- [16] Frank M. White, *Viscous Fluid Flow*, McGraw Hill Int. Edition., New York, 1991.
- [17] David Naylor and Patrick H. Oosthuizen, *Introduction to Convective Heat Transfer Analysis*, McGraw Hill Int. Edition., New York, 1991.
- [18] S. Roy Choudhury and Y. Jaluria, Analytical solution for the transient temperature distribution in a moving rod or plate of finite length with surface heat transfer, 1993.
- [19] Marvin J. Weber, Ph.D. *Handbook of Optical Materials*, CRC Press. University of California Berkeley. California, Boca Raton London New York Washington, D.C.
- [20] S. Kase and T. Matsuo, Theoretical analysis of melting spinning, *Journal of Text. Mach. Society of Japan*, vol. 18, No. 3, p. 188, 1965.